16

Fluorescent Calcium Indicators: *Subcellular Behavior and Use in Confocal Imaging*

Donald M. O'Malley, Barry J. Burbach, and Paul R. Adams

1. Introduction

Most animal cells maintain a large gradient of free calcium across the plasma membrane (10,000-fold or more), with intracellular free calcium held at a level of about 100 n*M*. To accomplish this, cells have an array of molecular machinery including ATP-driven calcium pumps, calcium exchangers, intracellular calcium storage compartments, and an assortment of calcium binding proteins ***(1–6)***. This machinery is needed because calcium is used ubiquitously as a signaling molecule, involving numerous receptors and a complex maze of intracellular signaling cascades ***(7–10)***. One approach to the study of this biological arena is the tracking of calcium levels in different subcellular regions. Our goal is to consider how fluorescent calcium indicators, in conjunction with confocal microscopy, can best be used to image subcellular calcium dynamics.

Calcium subserves critical functions in nerve and muscle cells. In skeletal muscle, e.g., calcium plays a pivotal role in muscular contraction, whereas in neurons, calcium triggers the release of neurotransmitters from nerve terminals ***(11–13)***. In the nervous system, calcium further regulates both gene expression and the excitability of neural networks and can also participate in the long-term storage of information. Fluorescent calcium indicators, which were developed largely through the efforts of Roger Tsien and his colleagues ***(14,15)***, provide a remarkable tool for looking at these processes. These indicators are especially useful when combined with a powerful imaging tool such as confocal microscopy. Our lab group has used confocal calcium imaging to visualize the distribution of functioning calcium channels, to study events occurring at the plasma and nuclear membranes, and as an in vivo probe of

From: *Methods in Molecular Biology, vol. 122: Confocal Microscopy Methods and Protocols*
Edited by: S. Paddock

neuronal activity ***(16–21)***. Although fluorescent calcium indicators are quite good at revealing the dynamics of intracellular processes, they are, paradoxically, not so good at telling us the absolute levels of free calcium at different subcellular locations.

The difficulty in determining absolute free calcium levels is well illustrated by an exchange of letters concerning findings from Stephen Baylor's group that were published in *The Biophysical Journal* ***(22,23)***. These letters debated the level at which free calcium rests in skeletal muscle and could come to no more agreement than to say that free calcium rests somewhere between 30 n*M* and 300 n*M*. A prime cause of this uncertainty is that calcium indicators behave very differently in vivo (inside cells) than they do in vitro (in cuvettes). At issue in these letters was a potentially dramatic shift in the indicator's intracellular dissociation constant (K_D). A further complication is that a calcium indicator's behavior can vary from one subcellular region to another—a situation that has led to the publication of some rather improbable "findings." The thesis of this chapter is that investigators must consider such complications if they hope to reach accurate conclusions about subcellular calcium dynamics. In reality, this is an extremely challenging problem without a robust, practical solution. However, achieving at least a partial understanding of an indicator's intracellular behavior will help, even if only to make clear the limitations of the technique. This chapter provides methods for: (1) assessing an indicator's behavior in "confocal cuvettes," (2) assessing the indicator's intracellular behavior, and (3) interpreting subcellular fluorescence gradients. To illustrate key issues that arise in subcellular calibration, this methodology is applied to some highly controversial nuclear/cytoplasmic fluorescence gradients.

2. Materials

2.1. Intracellular Solutions

2.1.1. Calibration Solutions

1. Zero Calcium:

ATP, disodium salt	2 m*M*
HEPES sodium	5 m*M*
$MgCl_2$	2 m*M*
TEA-chloride (tetraethylammonium)	20 m*M*
Gluconic acid	100 m*M*
Cesium hydroxide	100 m*M*
BAPTA	10 m*M*

   (Note: adjust final pH to 7.3 with NaOH)
2. High Calcium: (add to zero calcium solution, then check pH):

Calcium chloride	10 m*M*

   (and reduce gluconic acid and cesium hydroxide to 90 m*M*)

Table 1
Formulation of Calcium Series

Free Ca^{2+} (n*M*)	Total Ca^{2+} (m*M*)	Calibration Solutions *0* Ca^{2+}	10 m*M* Ca^{2+}	Bound Fluo 3	Predicted Fluor.
0	0.000	1000	0	0.00	100
1	0.062	994	6	0.25	114
7	0.421	958	42	1.74	199
35	1.803	820	180	8.08	561
62	2.807	719	281	13.48	868
177	5.284	472	528	30.78	1854
350	6.911	309	691	46.78	2766
700	8.204	180	820	63.75	3734
3,580	9.666	34	966	89.99	5229
7,330	9.888	12	988	94.85	5506
14,200	10.000	0	1000	97.27	5659
45,600	10.110	0	1000[a]	99.10	5749

This formulation is based on the calibration solutions specified in **Subheading 2.1.1**. 10 m*M* BAPTA and 100 m*M* fluo-3 are entered into the calculation program and the amount of Total Calcium (m*M*) is calculated by the program for each Free Calcium level (in n*M*) specified. The number of microliters of 0 calcium and high calcium solution to make 1 mL of each solution in the calcium series is also specified. At the same time that Total Calcium is determined from the program, the amount of calcium-bound fluo-3 (%) is also recorded. This is used to calculate the predicted fluorescence using $F = (100 - B) + 58B$.

[a]Because this calcium level exceeds the 10 m*M* calcium in the stock, add a small amount of extra calcium, 1.2 µL, from a 100 m*M* $CaCl_2$ stock solution.

2.1.2. Physiological Solution

Same as zero calcium solution, but remove BAPTA and increase gluconic acid and cesium hydroxide to 110 m*M*.

2.2. Calcium/BAPTA Mixtures

The makeup of a set of solutions with different levels of free calcium, i.e., a *calcium series* for evaluating fluorescent calcium indicators, is described in **Table 1.**

2.3. Imaging System (Main Components)

1. Bio-Rad MRC 600 (or other line-scanning confocal imaging system)
2. Zeiss IM 35 inverted microscope (or other inverted microscope)
3. Leitz 50X 1.0 NA water immersion objective (or other high throughput objective)
4. Newport vibration isolation table
5. UniBlitz external shutter (required for patch-clamping experiments)

2.4. Electrophysiology

2.4.1. Basic Patch Clamping (Main Components)

1. Axoclamp 2A patch-clamp amplifier
2. Tektronix storage oscilloscope
3. Leader monitor oscilloscope
4. WPI interval generator
5. Gould 2 channel chart recorder
6. Narashige aqua micromanipulator
7. Flaming-Brown micropipet puller, Sutter Instruments

2.4.2. Intracellular Perfusion (Additional Items)

1. Modified electrode holder A058-C, E. W. Wright
2. Internal perfusion tube, quartz, 200 µm outer diameter
3. Microcap micropipets, Drummond Scientific Co

2.5. Definitions

Two terms need to be distinguished:

1. *Cytoplasm*—the contents of the cell outside of the cell's nucleus, including *both* organelles and cytosol.
2. *Cytosol*—the "aqueous space" of the cytoplasm, i.e., the solution that surrounds the cytoplasmic organelles.

3. Methods

Fluorescent calcium indicators are typically loaded into cells via one of two main techniques: (1) direct "injection" of the indicator or (2) using the membrane crossing or acetoxymethylester or "AM"-form of the indicator. Within the injection category, we use an *electrophysiological* technique, patch-clamping, to load calcium indicators into nerve cells—either cultured cells or cells in brain slices. Although electrophysiology is not a trivial technique to acquire, it has the advantage of loading the fluorescent indicator directly into the aqueous space of the cell, i.e., the cytosol. The alternative, bathing cells in the membrane permeant "AM" form of an indicator, allows the indicator to cross the plasma membrane, after which it is metabolically trapped inside the cell by deesterification. *AM* indicators cross not only plasma membranes, but also organellar membranes which adds another level of complexity to subcellular calibrations (***24–29***; *see* **Note 1**). This chapter focuses on the simpler case of the non-AM indicators, i.e., the water-soluble forms: free acid, salt, and dextran-linked forms. This chapter also focuses on "single-wavelength" indicators, which are most widely used in confocal imaging, rather than the "ratiometric" indicators, where images are acquired at two wavelengths and used to generate a ratio-image (**Note 2**). The issues discussed pertain, however, to both AM and ratiometric indicators.

3.1. Formulation of Calibration Solutions

The *intracellular* solution (**Subheading 2.1.**) used in our patch-clamp pipettes is designed to mimic, to some extent, the intracellular milieux (**Note 3**). The baseline behavior of a fluorescent calcium indicator is first measured in a cuvette using the calibration version of our intracellular solution (**Subheading 2.1.1,**). The chief components of the intracellular solution are a physiological salt concentration, a pH buffer, ATP, magnesium, a calcium buffer, and the fluorescent calcium indicator. BAPTA is the calcium buffer of choice for our experiments because it is faster and less pH-sensitive than the other main calcium buffer, EGTA ***(30,31)***.

For calibration experiments, a high concentration of BAPTA, 10 m*M*, is used to "clamp" the concentration of free calcium either in vitro or inside cells. Free calcium is set at different levels by adding varying amounts of calcium to a 0 calcium/10 m*M* BAPTA solution. This calcium series (**Table 1, Subheading 2.2.)** spans the calcium-sensitive range of the indicator. The fluorescence of the indicator is then measured at these different calcium levels. A fixed concentration of calcium indicator (100 μ*M* in our experiments) is used with the calcium series to determine the K_D and dynamic range (maximal fluorescence response) of the indicator. In practice, the desired set of calcium levels is created by mixing together varying amounts of 0 calcium calibration solution and high calcium solution (10 m*M* total calcium). The required total calcium is first calculated and the relative mix of the 0 and high calcium solutions determined (**Table 1**).

The calculation of the total amount of calcium required to set free calcium at a specific level is not trivial, since multiple equilibria (calcium/BAPTA and calcium/indicator) must be solved. Bers et al. ***(31)*** describe a program that does this calculation based on an iterative procedure reported by Fabiato and Fabiato (***32***; *see* **Note 4**). Using this type of program, we enter the total amount of indicator (100 μ*M*) and a guess of its K_D (400 n*M* for fluo 3) plus the total amount of buffer (10 m*M*) and its K_D (160 n*M* for BAPTA) and the desired concentration of free calcium. The program then solves for the unspecified variable, in this instance total calcium. The uncertainty in the indicator's K_D is not a problem at this point because of the large excess of BAPTA. BAPTA's K_D, however, depends on salt concentration and temperature, both of which must be taken into account (**Note 5**). The set of calcium solutions described (**Table 1**) can be used to check successive batches of indicator or new indicators being tested. Although this might seem laborious (**Note 6**), one may wish to know, before completing a series of experiments, how responsive the calcium indicator is and whether or not its K_D is close to the advertised value (which may not be the case). These calibration solutions will also be used for

in vivo "calcium clamp" experiments, where the indicator's behavior is determined inside living cells. One shortcut for checking new batches of indicator is to measure the indicator's fluorescence at two calcium levels: 0 calcium and saturating (10 m*M*) calcium. Although this provides only a dynamic range, it at least gives a sense of the indicator's performance with a particular imaging system and under actual experimental conditions.

3.2. "Cuvette" Calibrations: Fluorescence vs [Free Calcium]

Fluorescent calcium indicators are expensive, so it is desirable to work with relatively small volumes. An alternative is to work with a low concentration of indicator during the calibration, but this deviates from the experimental condition so we avoid it. From a 20X stock of the indicator (2 m*M*, in de-ionized water), 10 µL of indicator is taken and added to 190-µL aliquots of the different calcium solutions (**Table 1**) in small (1 mL) plastic conical tubes and mixed well. A Bio-Rad MRC 600 with an inverted Zeiss microscope (**Subheading 2.3.**) was used to collect the fluorescent measurements shown in this chapter, but the methods are directly applicable to other confocal systems. Our "cuvette" consists of a small well that is fashioned by cutting a 14 mm diameter hole in the center of a 35-mm plastic petri dish and then gluing a square glass coverslip onto the bottom of the dish, covering the hole (**Note 7**). For calibration, a small droplet (4–5 µL) from each solution in the calcium series is placed on the coverslip. About five droplets can be conveniently spaced out across the coverslip, allowing the fluorescence at five calcium levels to be quickly determined. The top of the well is then covered with a coverslip to slow evaporation. The fluorescence of each droplet is then measured and its fluorescence plotted as a function of calcium concentration (**Note 8**). Our calibration of fluo-3, shown in **Fig. 1**, used 10 calcium levels.

The indicator's in vitro or "cuvette" behavior can now be evaluated. The K_D is simply read from the plot of fluorescence vs calcium concentration: the concentration that produced one-half of the total fluorescence increase is the K_D. To more completely evaluate the behavior of the indicator, the predicted fluorescence is also plotted vs calcium concentration. The determination of predicted fluorescence is based on the observed K_D and dynamic range. The calcium calculation program is used as described previously, except that the indicator's observed K_D, rather than the estimated K_D, is used. Keeping the total concentration of indicator fixed at 100 µ*M*, the amount of calcium-bound indicator is read from the program after entering each free calcium level (**Table 1**). Because fluorescence is directly proportional to the amount of calcium-bound indicator (after subtracting the 0-calcium fluorescence), the predicted fluorescence can be directly calculated. To standardize these calibration curves, the 0 calcium fluorescence (F_{min}) is normalized to a

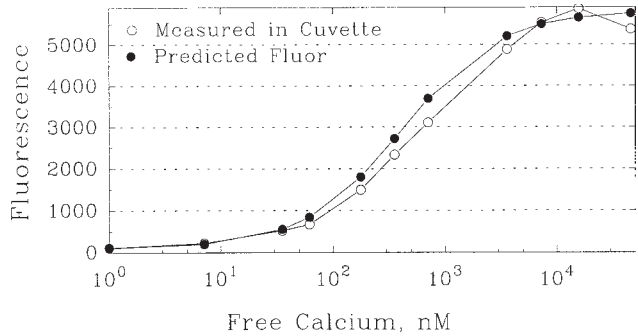

Fig. 1. Predicted vs observed fluorescence of fluo-3. The fluorescence of fluo-3 is measured in microliter-droplets placed on a glass coverslip. The droplets have varying concentrations of free calcium, as described in **Subheading 2.2.** Measurements are made with the MRC 600's aperture set at 1/3 open and with a 1.5 log unit neutral density filter. The gain of the photomultiplier tube was initially set at maximum for the zero calcium solution, but with increasing calcium (fluorescence) levels, was adjusted downward in 1 unit increments to accommodate the range of fluorescence values encountered. Fluorescence values are then scaled to the initial gain setting after determining gain correction factors based on the use of test droplets and test slides as fluorescence standards.

value of 100 and the maximum fluorescence (F_{max}) is then the maximal-fold change observed x 100, yielding a value of 5800 for the 58-fold dynamic range of fluo-3. For **Fig. 1** the predicted fluorescence curve is calculated from:

$$F = (100 - B) + 58 \cdot B \qquad \text{(Eq. 1)}$$

where B = the percentage of calcium-bound fluo-3 and is equal to the amount of fluo-3 bound, in μ*M*, determined by the calculation program (**Table 1**).

In a perfect world the calculated and the observed curves would match exactly. As seen in **Fig. 1**, there was fair agreement between the predicted and the observed fluorescence using fluo-3's published K_D of 400 n*M*. One could attempt to better fit the predicted curve to the observed fluorescence by, e.g., varying the value for fluo-3's K_D in the program and recalculating the fraction bound and the predicted fluorescence. However, an indicator's intracellular behavior deviates so greatly from its in vitro behavior that small refinements in the cuvette value have little biological relevance.

3.3. Intracellular Calibration

The calcium binding and spectral properties of fluorescent calcium indicators are dramatically altered by the intracellular milieux. In muscle cells, perhaps 85% of the indicator is bound to proteins or other large molecules,

resulting in an increase in the K_D of three- to fourfold ***(11,33)***. This appears to be true for most fluorescent calcium indicators, including fura-2, indo-1, fluo-3, and fura red ***(34–36)***. Also the indicators have a substantially reduced dynamic range intracellularly, versus their dynamic range in cuvettes ***(34,36,37)***. Furthermore, spectral shifts can result from indicator/protein interactions and other causes ***(34,38–42)***. Spectral shifts may be especially problematic for ratiometric indicators because a small shift in fluorescence spectra could have a much larger effect on ratio imaging than on single-wavelength imaging. Even greater problems are caused by compartmentalization of indicators into cytoplasmic organelles, such as the endoplasmic reticulum and mitochondria, which often contain high levels of free calcium. In such cases, the cytoplasmic fluorescence (or cytoplasmic ratio) is the sum of organellar plus cytosolic fluorescence, whereas the nuclear fluorescence (or ratio) has no organellar contribution and therefore will not equal the cytoplasmic fluorescence. This is quite a serious complication for the membrane permeant or AM form of indicators because AM-indicators may cross intracellular membranes just as readily as they cross the plasma membrane ***(25,26,28,29,43)***. For example, in cardiac ventricular cells, mitochondria were reported to contain roughly 50% of the indo-1 AM taken up by the cell ***(43,44)***. A final complication is the differential binding of calcium indicators to the assorted constituents of different subcellular regions (e.g., different proteins, DNA, etc.). In aggregate, these issues make it almost a foregone conclusion that the calibration curve will vary from one subcellular region to another. These complications apply to both single-wavelength and ratiometric calcium imaging (**Note 9**).

The standard approach to intracellular calibration of fluorescent calcium indicators is to bathe cells in a second class of membrane permeant compound—the calcium ionophores such as ionomycin and A23187. These ionophores facilitate equilibration of calcium levels across the membrane. This approach seems to work well on some cell types but less well on others—the ionophores may work very slowly and may not fully equilibrate calcium across the plasma membrane ***(27,45,46)***. Ionophores are especially difficult to employ when working with tissues such as brain slices. In addition, if there is compartmentalized indicator, the ionophores might also cause redistribution of calcium between different compartments and affect other ionic gradients and pH, all of which can alter the behavior of the indicator ***(26,38,47)*** and influence the calibration. It is thus perhaps not surprising that few detailed intracellular calibration curves have been published for fluorescent calcium indicators. Work by Blatter and Wier ***(43)*** and Schnetkamp et al. ***(48)*** provided detailed calibrations using batches of either permeabilized cells or rod outer segments, respectively, but we are aware of no subcellular calibration where a detailed series of calibration images, collected from a single cell, has been presented. The

majority of calcium imaging studies either use in vitro calibration data or simply avoid estimating calcium concentrations altogether and report only fluorescence values. In this chapter, we will focus on alternative calibration approaches that rely on patch clamping. Although these approaches encounter some of the same limitations as the ionophore approach, they appear to have some advantages.

Two distinct electrophysiological approaches can be used to attempt intracellular calibration of calcium indicators: calcium pulsing and intracellular perfusion. Calcium pulsing involves patch-clamping cells (**Note 10**) and then using depolarizing voltage pulses to flood the cell with calcium. Intracellular perfusion also uses patch-clamping with the additional use of a fine tube that runs inside the patch-clamp electrode down to the tip; this tube is connected to a valve and allows perfusion of the pipette tip (and hence the cell) with any desired solution. Intracellular perfusion is substantially more difficult than calcium pulsing, but has clear advantages. In the context of these two calibration approaches, we will consider a particularly controversial topic: the existence of persistent calcium gradients that span the nuclear envelope. This ongoing controversy is deeply intertwined with the problem of subcellular calibration of fluorescent calcium indicators. It therefore provides a framework within which to discuss the interpretation of confocal calcium images.

3.3.1. Calibration via Intracellular Perfusion

In a typical experiment, the fluorescent indicator is dissolved in intracellular solution (**Subheading 2.1.**) and injected into a patch-clamp pipet. The patch-clamp pipet is then pushed against the cell membrane, forming a high-resistance seal. The small patch of membrane under the tip of the pipet is ruptured by gentle suction. This allows the contents of the pipette to diffuse into the cell. The intracellular solution in the pipette will gradually replace the cell's cytosol, i.e., the aqueous space of the cell outside of the organelles. This is why the solution is designed to mimic, to some extent, the intracellular milieux (**Note 3**). For all calibration experiments, calibration solution (**Subheading 2.1.1.**) is used; it has a high concentration of BAPTA to allow the setting of free calcium at a particular level. For intracellular perfusion, the patch electrode is initially filled with one solution (solution A) and after filling the cell to (or near) equilibrium with indicator (**Note 11**), the pipet tip is perfused with a second solution (solution B). The intracellular perfusion apparatus is set up by threading a fine piece of inflow tubing through a rubber O-ring into the patch-clamp electrode holder (**Note 12**). A fine quartz inner pipette fits snugly into this inflow tubing and extends very close to the tip of the patch pipet, which is filled with solution A. From the pipet, the inflow tubing runs to a reservoir filled with solution B. The electrode holder also has a port with a small tube running to an

outflow chamber. This outflow line is clamped and held under a modest vacuum during the process of patch-clamping. At a given point in the experiment, the inflow line is unclamped and the vacuum from the outflow line then begins to pull solution B through the system. Once the reservoir is drained and the patch-electrode filled with solution B, the lines are re-clamped. By this point, solution B has begun diffusing into the cell.

Filling a cell with a 0 calcium solution (solution A) and subsequently perfusing it with a saturating calcium solution (solution B) provides the intracellular dynamic range of the indicator. That is, by taking an indicator from a calcium free to a calcium-saturated state, the maximal possible intracellular fluorescence change is obtained (**Note 13**). A key advantage of this style of calibration is that the only thing that is directly changed is the cell's free calcium concentration. This approach was illustrated for fluo 3 using cultured bullfrog sympathetic neurons (*see* Fig. 7A in **ref. *20***). In that study, the indicator showed a 24-fold fluorescence increase in the nucleus and an 18-fold increase in cytoplasm. This is the largest intracellular dynamic range demonstrated for fluo-3 in a calcium imaging study, which suggests that this method of controlling calcium may be as effective as other methods. In this calibration, the nucleus was initially twice as bright as the cytoplasm. This could be interpreted either as a simple fluorescence gradient or as a resting nuclear/cytosolic calcium gradient. Because intracellular perfusion produced roughly parallel fluorescence increases in both the nucleus and cytosol across a broad range of calcium levels, it seems much more likely that the resting fluorescence gradient is due to the behavior of the indicator, rather than to a nuclear/cytosolic calcium gradient that persists across all calcium levels (**Note 14**).

Confocal microscopy is a key tool for making such subcellular measurements accurately. Even in the case of the large-sized bullfrog neurons used here, good optical sectioning is needed to ensure that the nuclear signal is not contaminated by signal from the overlying cytoplasm. **Figure 2** shows two confocal views of a cell: a conventional "XY" image (**Fig. 2A**) and a vertical slice through the cell (referred to as an "XZ" image; **Fig. 2B**). The XY image shows an example of the nuclear and cytosolic regions from which our measurements are typically made. The XZ image is made by successively scanning a single line in the XY plane while focusing the objective at successive planes spanning the vertical (or "Z") extent of the cell. The XZ scan illustrates the optical sectioning achieved. In this instance the nucleolus (the bright spot in the center of the nucleus), which is only about 4 μm in diameter, is well-resolved. Few studies on nuclear calcium signals have so directly illustrated actual optical performance. This is unfortunate because XZ scans make it easy to graphically document said performance.

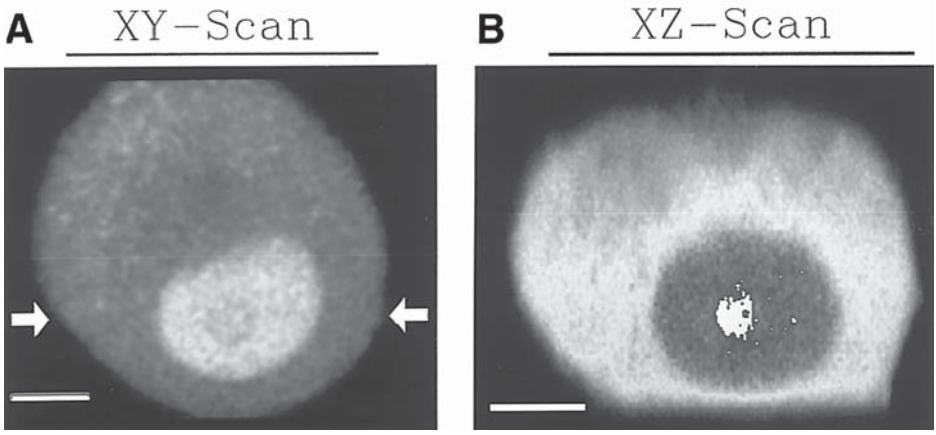

Fig. 2. Top and Side views of a cultured sympathetic neuron. In the conventional top view **(A)** the nucleus (bright region between the arrows) is easily distinguished because of its brighter fluorescence. This pattern of labeling always occurs when fluorescent calcium indicators are loaded into the aqueous space of nerve cells. A side view or "XZ"-scan **(B)** is generated by repetitively scanning a single line, in this instance, the line running between the two arrows in (A), while the lens is focused through the vertical or "Z" extent of the cell (lines were acquired at 0.4 µm intervals, with a total of 120 Z-steps). The scale bars are 10 µm; in (B) the scale bar is positioned at the level of the coverslip on which the cell is resting. All images in this chapter are linearly contrast enhanced except for the image in (B) which is a nonlinear representation provided only to highlight anatomical details such as the nucleolus—the small bright dot in the center of the nucleus (the nucleolus is 15% brighter than the nucleus which in turn is twice as fluorescent at the cytoplasm, the nucleus appears darker in this rendering because of the nonlinear contrast enhancement).

The combination of optical sectioning and intracellular perfusion thus confirms that the nucleus and cytoplasm show parallel fluorescence increases across a broad range of calcium levels. One might argue, however, that the calcium indicator was not saturated with calcium since it did not exhibit the full dynamic range observed in cuvettes. If so, then cytosolic calcium could, in theory, rest at one-half of the nuclear calcium level, show a 20-fold increase, and still be at a level far from saturating the indicator (thus preserving the idea that the nuclear signal is amplified relative to the cytosolic calcium signal). This is very unlikely because of the large size of the nuclear response, as well as the limited intracellular dynamic range of calcium indicators and the initial starting conditions (**Note 15**). Intracellular perfusion provides an even more compelling criticism of this idea. In Fig. 7b from **ref. *20***, a cell is initially filled with low calcium solution and is then perfused with 10 m*M* manganese, a concentration that is about 1,000,000-fold greater than fluo-3's K_D for manganese

(8 n*M*). This causes a rapid, parallel increase in both nuclear and cytoplasmic fluorescence (about 5.5-fold) that quickly saturates, virtually eliminating any plausible gradient hypothesis (in cuvettes, manganese produces an eightfold fluorescence increase when it binds to fluo-3; **ref. *49***). Again the nuclear/cytoplasmic ratio is about two, supporting the previous contention that calcium had saturated the indicator in both compartments of the cell. In addition, the time course required for manganese to saturate fluo-3 was similar, in both compartments, to that of calcium. In total, these findings provide powerful evidence that the nucleoplasm is in free communication with the cytosol (insofar as small molecules are concerned) and that nuclear and cytoplasmic fluorescence signals must be independently calibrated. These findings are supported by reports from other labs ***(50–54)*** and by earlier work from our lab ***(17)***.

There are several factors that probably contribute to the resting nuclear/cytoplasmic fluorescence gradient. First, the cytoplasm is packed with membrane bound organelles, which will tend to exclude the highly charged potassium salt form of fluo-3 (it has a charge of -5). In the "nucleoplasm," there are no membrane bound organelles, so there is no "excluded" volume in the nucleus. In the cytoplasm, even with confocal calcium imaging, it is generally not possible to resolve the interstitial aqueous space (cytosol) from the organelles. Hence, the cytoplasmic signal is an integration of fluorescence coming from regions with fluo-3 (cytosol) and regions that are largely without fluo-3 (organelles). A second possible cause of nuclear/cytoplasmic differences is differential binding of fluo-3, including the possible intercalation of molecules such as fluo-3 into DNA ***(55)***. Lastly, other aspects of the nuclear environment may enhance the fluorescence of fluo-3 ***(54)***. Enhanced nuclear fluorescence is not restricted to calcium indicators because other dyes such as DAPI and lucifer yellow also show bright nuclei. Evaluating the competing explanations for the brighter nuclear signals is not trivial, so questions about these persistent subcellular fluorescence gradients are likely to persist.

With intracellular perfusion, the indicator's behavior was imaged in both compartments at essentially all calcium levels ranging from 10 n*M* to saturating calcium levels. Only 16 discrete time points (or "calcium levels") were sampled, but more could have been. This gives a comprehensive picture of how the indicator behaves in different subcellular regions across nearly the full range of calcium levels to which the indicator is responsive. This has not been directly illustrated (to our knowledge) in other calcium imaging studies. Those studies that take the effects of the intracellular environment into account typically provide a minimum fluorescence (F_{min}), a maximum fluorescence (F_{max}) plus one intermediate point for the K_D calculation. Indeed, we are not aware of the actual fluorescence images being shown for even these three points—in any study. With our calibration approach, the only factor that was directly

changed inside the cell was the concentration of calcium in the aqueous space. One concern with a traditional calibration is how an amphipathic compound such as the ionophore will affect the stability of the plasma membrane. A related problem is that the fluorescence increase produced by high calcium plus A23187 or ionomycin is not always maximal ***(27,45,56)***. Digitonin, a stronger permeabilizing agent, can yield a substantial further fluorescence increase of the calcium indicator, but also leads to leakage of indicator out of the cell. This seriously impedes calibration ***(45,57)***. It would be instructive to compare calcium images generated via ionophoric calibrations to those produced by the electrophysiological approach so as to determine which protocol yields the largest and most systematic changes in subcellular fluorescence levels.

A particularly desirable feature of any calibration approach is reversibility. In the calibration mentioned ***(20)***, the "electrical" health of the cell declined as intracellular calcium and manganese reached toxic levels. Although cells may look fine anatomically, a decline in their input resistance suggests a deteriorating plasma membrane. For smaller calcium changes, however, the effects of intracellular perfusion are reversible, as shown in a study of calcium-modulated potassium channels, where calcium was taken from 0 n*M* to 120 n*M* and back to 0 n*M* without any apparent ill effect on the potassium current or the health of the cell (*see* Fig. 2 in **ref. *18***). Such reversibility has generally not been evident in ionophoric calibrations. Intracellular perfusion, by virtue of its reversibility and noninvasiveness, is thus a potentially powerful technique for subcellular calibration of fluorescent indicators. Although technically challenging, this approach is also a general means to sequentially introduce impermeant compounds into cells at relatively defined concentrations during calcium imaging experiments. This approach may therefore have other applications.

3.3.2. Calibration via Calcium Pulsing

A technically less demanding calibration is to clamp free calcium at one concentration (by filling the cell via the patch-clamp electrode) and then take advantage of the cell's calcium channels to flood the cell with calcium, thereby saturating the calcium indicator. Nerve cells generally have a large complement of somatic calcium channels, so once a patch-clamp seal has been obtained and the cell filled with indicator, voltage-clamp can be used to repetitively deliver pulses of calcium (**Note 16**). To determine the dynamic range of the indicator, the cell is initially filled with 0-calcium solution and pulses of calcium are administered until the indicator is saturated (**Fig. 3**). One problem is that calcium channels tend to run down (inactivate) over time, limiting the ability to administer calcium. This makes it difficult to ensure that the indicator is saturated with calcium. The size of the calcium current, however, is continuously monitored during the calibration. If the voltage pulses are still

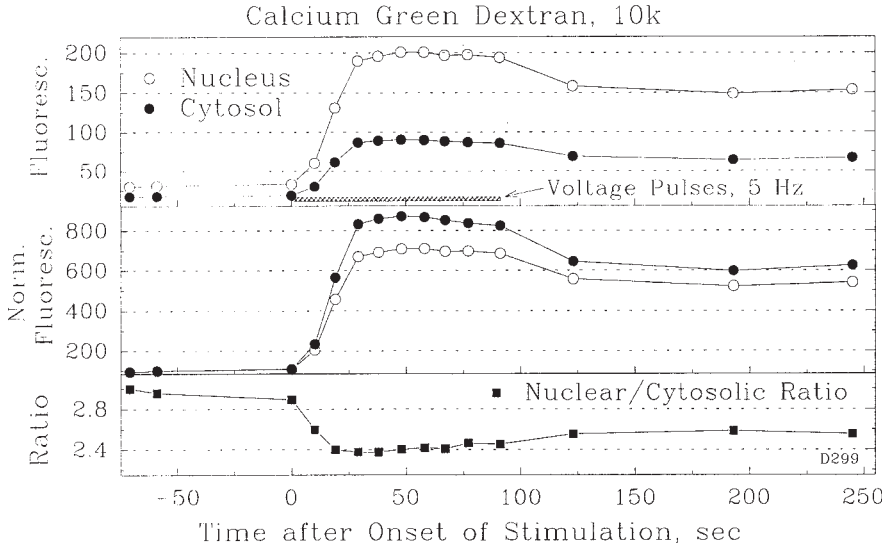

Fig. 3. Intracellular dynamic range of calcium green dextran (CGD). The neuron is loaded with a 0 calcium/10 m*M* BAPTA solution containing 100 µ*M* CGD (10,000 Mr). The cell is voltage clamped at –70 mV and filled with CGD for approx 7 min prior to stimulation. At time 0, depolarizing voltage pulses (**Note 16**) are used to flood the cell with calcium. Fluorescence rapidly plateaus in both nucleus and cytosol, with a very similar time course. The fluorescence increases more in the cytosol than in the nucleus—a phenomenon that is usually observed with dextran-linked calcium indicators (the reverse is true with low molecular weight indicators). A slight recovery of the fluorescence toward baseline is observed after cessation of the voltage pulses, but cultured nerve cells seem to have difficulty in removing the very large quantities of calcium administered by this type of saturation protocol.

admitting appreciable quantities of calcium when the fluorescence reaches a plateau, which in this instance occurred about 25 s into the stimulation period, it suggests that intracellular calcium has surpassed the level required to saturate the indicator.

Another potential complication is that the calcium influx induced by the voltage pulses may be countered by an equal calcium efflux. Calcium extrusion mechanisms tend to be an order of magnitude or more slower than the peak influx mechanisms, so this seems unlikely. But, at high calcium loads, it is possible that Na^+/Ca^{2+} exchangers may produce a high efflux rate (**Note 17**). One control for this is to simply remove extracellular sodium (by, e.g., replacement of sodium with n-methyl glucamine). If the indicator is not already saturated, then halting sodium influx, which drives the largest component of calcium extrusion, should cause an immediate reduction in calcium efflux and

a concomitant fluorescence increase. Alternatively, one could vary the extracellular concentration of calcium (normally 2 m*M* in our studies) between 0.5 and 10 m*M*. Any calcium level within this range of concentrations is sufficient to saturate the higher affinity calcium indicators discussed here (fluo-3, calcium green, oregon green-BAPTA ,and their dextrans), so the maximum obtainable fluorescence increase should not be greatly affected by changing extracellular calcium over this range once the indicator is saturated. If, however, calcium extrusion is preventing saturation, then voltage pulses at the higher concentrations of calcium should counteract extrusion, to some extent, and thus increase the observed dynamic range.

To estimate the indicator's intracellular K_D, calibration solutions are used to clamp calcium at intermediate calcium levels After setting intracellular calcium at each level, the indicator is subsequently saturated by calcium pulsing. The fluorescence responses determined for each starting calcium level allow independent estimates of the indicator's K_D to be made (**Note 18**). **Figure 4**, for example, shows a series of determinations of the intracellular K_D of calcium green dextran (CGD, 10,000 Mr), an indicator that provides robust, stable responses and has been quite useful for studying calcium dynamics in rat brain slices ***(16)*** and living zebrafish ***(21,58)***. In this series, calcium is clamped at 3 intermediate levels and the maximal fluorescence response is determined for each starting level. For each calcium level, the experiment is repeated on several cells and the maximal fluorescence increase obtained is used to determine the K_D. There are trivial reasons for getting smaller than maximal fluorescence changes (such as failure of the calcium current or loss of cell integrity), so the largest observed change is taken as the true maximal fluorescence increase. For the three calcium set points used (10 n*M*, 107 n*M*, and 369 n*M*) the K_D determinations were, respectively: 100, 230, and 320 n*M* (**Note 19**). The low value (associated with the 10 n*M* set point) was partially discounted because of the greater error associated when correcting for autofluorescence and black level at very low starting fluorescence/calcium levels. The two higher values were closer to calcium green dextran's in vitro K_D of 250 n*M*. Taking a weighted average of the three determinations thus yields a value in agreement with the published K_D. This value was therefore used for our intracellular calcium measurements. One caveat is that while dextran-linked indicators show the least compartmentalization, and should be least influenced by the intracellular environment, they have been reported to undergo an up to twofold increase in K_D in muscle cells ***(57)***. Given the uncertainty in our intracellular determinations, it would be most prudent to assume that CGD's K_D in neurons is somewhere between 100% and 200% of its in vitro value.

In cells lacking robust calcium channels, alternative schemes of flooding cells with calcium are possible, including different combinations of the follow-

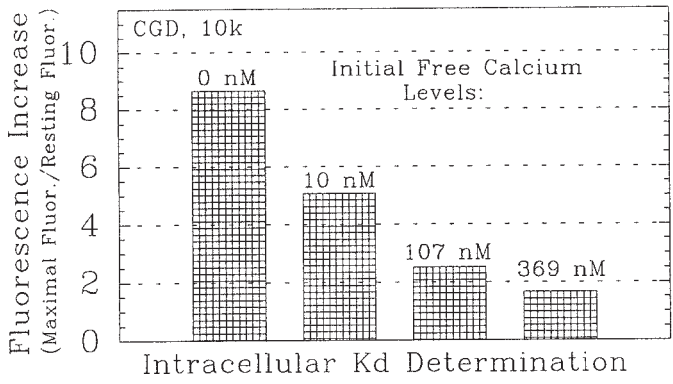

K_D Determination Parameters

Free Ca^{2+} nM	Fluoresc. Increase Max/Init.	Relative Starting Fluoresc.	Est. Ca^{2+}-Bound Fluo-3, %	Apparent K_D nM
0	8.65	100	0	-
10	5.07	171	9.3	100
107	2.52	343	31.8	230
369	1.66	521	55.0	320

Fig. 4. K_D determination. Cells are filled with calibration solution containing intermediate levels of free calcium (**Table 1**). The maximum fluorescence increase produced by calcium pulsing is shown for four different starting calcium levels. The value for the fluorescence increase (final fluorescence/resting fluorescence) is shown in the accompanying table along with a calculated "absolute" starting fluorescence that assumes the indicator is saturated after calcium pulsing (*see* text; this value is scaled to a 0 calcium value of 100). The amount of calcium-bound CGD corresponding to the calculated starting fluorescence is shown. The K_D is then determined iteratively for each intermediate calcium level using a calcium calculation program (*see* text for further details).

ing: high potassium, calcium-channel activators, blockers of the calcium pump or the Na^+/Ca^{2+}-exchanger, receptor agonists and releasers of intracellular calcium stores. The specific approach can be tailored towards the particular cell type being imaged. This calcium-clamp approach to determining intracellular K_D is equally applicable to the intracellular perfusion technique, where solution A is an intermediate calcium level and solution B a saturating level of calcium. The more robust nature of intracellular perfusion could make it better suited for calibrating higher K_D indicators, such as furaptra and calcium green 5N ***(37,59–61)***. Although this calibration approach is unorthodox, it appears to be least disruptive of the intracellular environment while providing a degree of

control over intracellular calcium levels that approaches or, at least in some cell types, exceeds that provided by calcium ionophores.

3.3.3. Construction and Use of Intracellular Calibration Curves

The standard equation for converting fluorescence values to calcium concentrations (for single wavelength indicators) is:

$$[Ca^{2+}] = K_D \cdot (F - F_{min})/(F_{max} - F) \qquad \text{(Eq. 2)}$$

where F_{max} = maximum fluorescence (i.e., calcium-saturated fluorescence), F_{min} = minimum fluorescence (0 calcium fluorescence), and F = the fluorescence value to be converted to a calcium concentration ***(46)***. This equation can be used directly if one has F_{max} and F_{min} for each cell studied. In practice, it may be difficult or impossible to determine F_{max} and F_{min}. This is especially true for cells in brain slices or intact animals. In such cases, it is not known where the experimental fluorescence values fit within the overall dynamic range of the indicator (F_{min} to F_{max}), i.e., resting calcium is not known. In this situation, the simplest approach is to assume a resting value of calcium and equate the cell's resting fluorescence to it (**Note 20**). For CGD, using the estimated intracellular K_D of 250 n*M* and an arbitrary value for F_{min} of 100 (resulting in an F_{max} of 870 for CGD's 8.7-fold intracellularly determined dynamic range) the curve in **Fig. 5A** is generated (**Note 21**). If a resting calcium value of 100 n*M* is assumed, the standard curve yields a resting fluorescence (F value) of 320. Thus, 320 is the fluorescence value to which the experimental resting values will be normalized. A scaling factor is then determined to scale all of the experimental values to the standard curve. For example, if resting fluorescence in the cytoplasm is 32 arbitrary fluorescence units (after correcting for autofluorescence and/or black-level), then the scaling factor would be 10, i.e., all cytoplasmic fluorescence measurements are multiplied by 10 and substituted directly into equation 2 to calculate the corresponding calcium levels. The nuclear scaling factor would obviously be different. If resting nuclear fluorescence were 64, then the scaling factor for nuclear measurements would be 5. For this analysis, the 8.7-fold maximal fluorescence increase observed in the nucleus (**Fig. 3**) was used to set the dynamic range. For a more rigorous determination, a separate dynamic range would be used for nucleus and cytosol. For simplicity, just the nuclear calibration curve is used here.

This calibration curve can be replotted in an instructive form: calcium is plotted vs $\Delta F/F$ for a series of different resting calcium levels (**Fig. 5B**). For each resting calcium level to be plotted, the initial point on the curve is the resting calcium level (e.g., 50 n*M*) and the resting $\Delta F/F$ is equal to 0, because there is no ΔF yet. But there is a resting fluorescence level, which is read from the curve in **Fig. 5A** (or calculated using the equation). For example, a resting

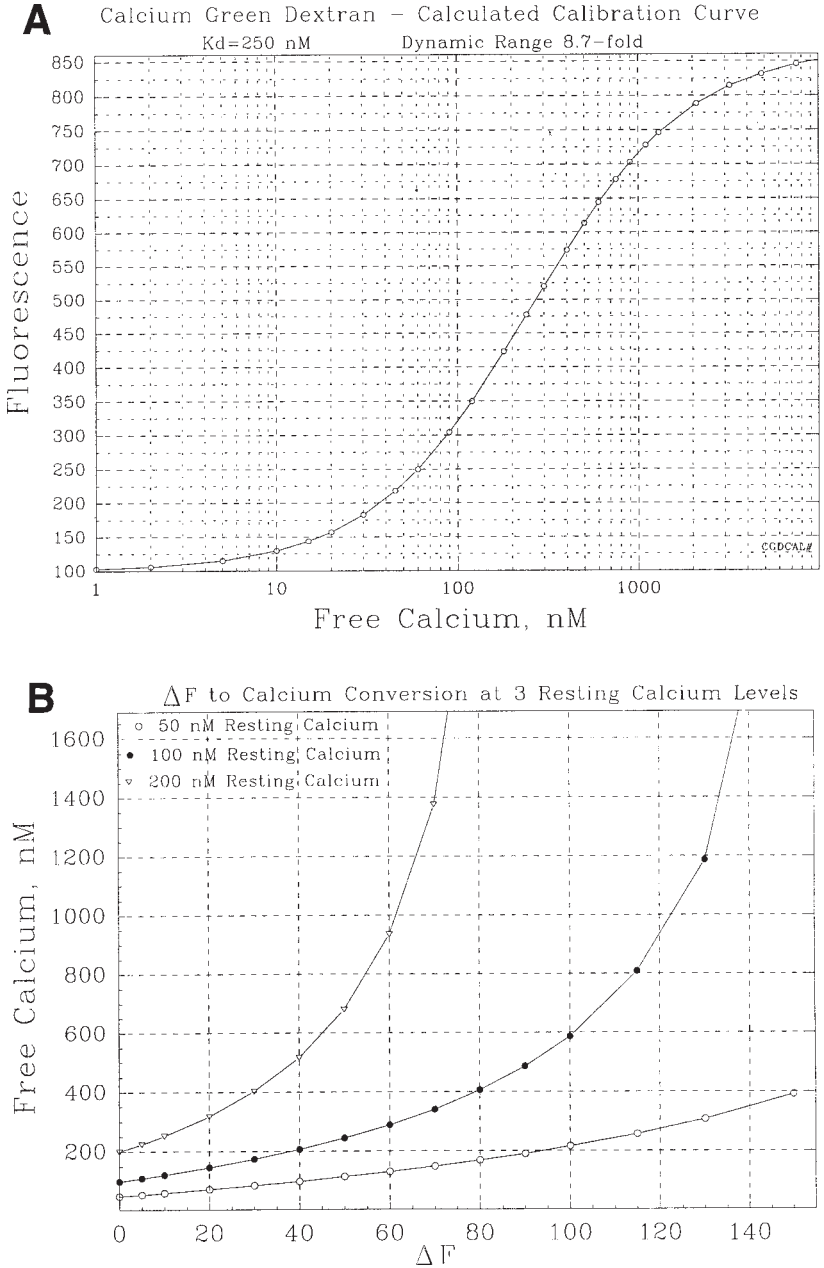

Fig. 5. Intracellular calibration curves. Based on the observed dynamic range and estimated intracellular K_D, fluorescence is plotted as a function of free calcium **(A)**. This curve is generated by choosing different calcium levels and using the calculation program to determine "*B*", the percent of CGD with calcium bound. Fluorescence is

calcium of 50 n*M* has a fluorescence value of 228 in arbitrary units. All subsequent values for the 50 n*M* curve in **Fig. 5B** are calculated by incrementing the fluorescence by a specific ΔF, calculating the total fluorescence produced by that fluorescence increase ($F_{REST} + \Delta F$) and entering that total fluorescence into Eq. 2 to calculate free calcium. For example, on the 50 n*M* curve, a 20% $\Delta F = 0.2 \times 228 = 45.6$. The total $F = 228 + 45.6 = 273.6$ This total is entered into eq. 2, with $F_{max} = 870$ and $F_{min} = 100$, yielding a calcium level of 73 n*M* for a $\Delta F = 20$. Curves were generated for three different resting calcium values: 50, 100, and 200 n*M*. These values all fall within the current "range of uncertainty" of neuronal resting calcium levels. The utility of this type of graph is that one can enter the graph with any relative fluorescence increase ($\Delta F/F$) and directly read out the size of the calcium response. More importantly, one can do this for each resting calcium level that one wishes to consider. For example, if one assumes a resting calcium level of 50 n*M*, then a $\Delta F/F$ of 60% would equate to a 90 n*M* increase in free calcium. In contrast, if resting calcium is assumed to be 200 nM, then a 60% $\Delta F/F$ equates to a 700 n*M* increase in calcium.

Such calculations may seem esoteric, but this analysis had a significant impact on the interpretation of calcium signals generated by the low-threshold (LT) and high-threshold (HT) calcium channels found on thalamic relay cells in rat brain slices ***(16)***. In that study, opposite conclusions were reached about the relative distribution of these two calcium channel subtypes, depending on whether a resting calcium of 50 n*M* or 100 n*M* was assumed. This ambiguity was due to a combination of the nonlinear relationship between calcium and fluorescence and the fact that different sizes of somatic fluorescence responses had been obtained in that particular experiment (**Note 22**). Although an exact answer on calcium channel distribution awaits further experimentation, had we not attempted to convert the raw fluorescence signals into calcium concentrations, we would have been unaware of the ambiguity inherent in the raw fluorescence data. In this particular instance, a simple change in protocol eliminates the source of ambiguity: the stimulus used to activate the channels is

---

then calculated from the equation $F = (100 - B) + 8.7B$. Alternatively, one could generate the curve by simply choosing fluorescence values and calculating free calcium directly from **Eq. 2**, where $F_{min} = 100$ and $F_{max} = 870$. **(B)** To illustrate the influence that resting free calcium level has on the interpretation of fluorescence responses, free calcium is plotted vs ΔF for several different resting calcium levels. To construct these curves, F is determined for a given resting calcium level from the calculation program or by trial and error usage of **Eq. 2**. The calcium values corresponding to different ΔF's are then calculated by calculating a total F value ($F_{REST} + \Delta F$) and then substituting that total F value into **Eq. 2**.

adjusted so that equal-sized somatic responses are produced for both channel types. With this modification, the relative direction in which the LT and HT calcium channel distributions are changing is clear regardless of the level of resting calcium. This approach thus provides the simplest starting point for the quantitative imaging of the distribution of functional calcium channels.

3.4. Indicator Comparison

Each calcium indicator seems to have its own unique "personality" owing perhaps to quirks in binding and compartmentalization. Rhod-2, e.g., exhibits a rather unique fluorescence pattern in that not only is the nucleus brighter than the cytoplasm, but the nucleolus is much brighter than the nucleus proper (**Fig. 6A**). It seems rather improbable that the nucleolar/nuclear fluorescence gradient reflects a standing calcium gradient. More likely, rhod-2 binds avidly to nucleolar constituents, or its fluorescence is enhanced by the nucleolar environment or some combination of both occurs. Calibration of rhod-2 by calcium pulsing shows that all three regions of the cell increase in parallel, with the nuclear and nucleolar signals showing relatively similar $\Delta F/F$ values, and the cytosolic signal reaching a much lower plateau (**Fig. 6B**). The large parallel increases observed in all compartments is far more easily explained as a quirk of the indicator rather than by a set of highly unusual calcium gradients maintained over a wide range of calcium levels. Indeed, the lack of a membrane around the nucleolus would seem to make it physically impossible for a nucleolar/nucleoplasmic calcium gradient to persist (**Note 23**), yet a nucleolar/nucleoplasmic fluorescence gradient was described as a calcium gradient in a study of cultured rat DRG neurons ***(62)***.

The maximum fluorescence increase shown by rhod-2 in vivo was much less than its response in cuvettes. This was true for all indicators whose intracellular dynamic ranges were determined in calcium pulsing experiments (**Fig. 7**; note that for several newer indicators, just the cuvette values were determined). It can be seen that the cuvette behavior approaches the intracellular behavior most closely for CGD, with fluo-3 being next closest and rhod-2 showing the most deviation. Compartmentalization of the indicators seems to play a role in the decreased dynamic range of both rhod-2 and fluo-3. For example, fluo-3 showed a 24-fold fluorescence increase in the nucleus and only an 18-fold increase in the cytosol (Fig. 7 in **ref. *20***). Such a result is consistent with a gradual internalization of the indicator into organelles which would leave some

---

Fig. 6. Intracellular behavior of Rhod-2. **(A)** After filling a cell with 80 μ*M* rhod-2 dissolved in 0 calcium solution (with 10 m*M* BAPTA; "low calcium"), the delivery of calcium pulses causes fluorescence to increase in the cytoplasm, nucleus and nucleo-

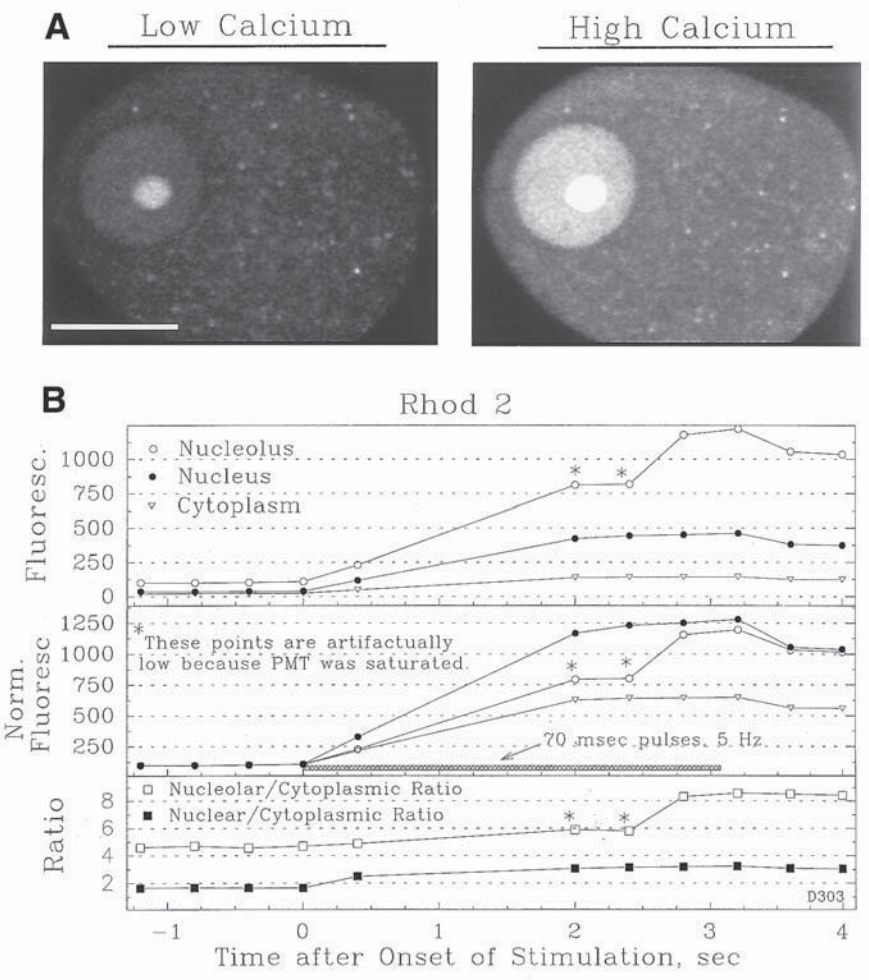

lus ("high calcium"). **(B)** All three regions increase in parallel, consistent with free diffusion of calcium throughout the aqueous space of the cell. As seen with fluo-3, the nuclear and nucleolar signals increase more than the cytoplasmic signal. Rhod-2 is unique, however, in that its nucleolar signal is twice as bright as the nuclear signal, even at the outset of the experiment (i.e., at a time when the cell is in excellent physiological condition). This nuclear/nucleolar fluorescence gradient is maintained across all calcium levels which argues against the idea of a "nuclear/nucleolar calcium gradient." Note that the nuclear/cytosolic fluorescence ratio reaches a higher value than is observed with fluo-3. This may be due to the reported accumulation of rhod-2 into mitochondria. Scale bar = 15 μm.

of the cytoplasmic indicator in a high-calcium (organellar) environment, where it would not respond to increasing cytosolic calcium levels. This would there-

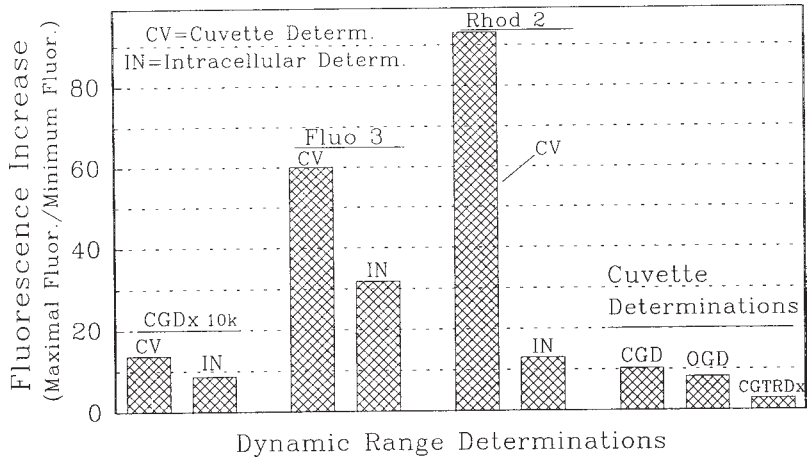

Fig. 7. Indicator Comparison: in vitro vs in vivo behavior. All three indicators tested intracellularly showed a decreased in vivo dynamic range, relative to their in vitro or cuvette value. This was most marked for rhod-2, whose intracellular dynamic range is reported for its nuclear response—its cytosolic dynamic range is even less. Fluo-3 showed the largest intracellular response but this can decline over time perhaps because of compartmentalization and gradual extrusion from the cell. The indicator manufacturers have not yet succeeded in producing a dextran-linked version of fluo-3, a compound that would constitute a major advance for calcium imaging. Cuvette determinations are shown for several newer indicators including Oregon green dextran BAPTA-488 (OGD) and a calcium green Texas red dextran conjugate (CGTRD). In preliminary in vivo studies, OGD was quite bright and yielded responses similar to CGD. In contrast, the cuvette behavior of CGTRD was disappointing and so it was not used inside cells. Our more recent batches of CGD (shown with the other cuvette determinations) have yielded somewhat smaller responses than previous batches, but it is not known whether this is due to the indicator itself or to other factors such as changes in the calibration solutions or imaging system.

fore decrease the cytoplasmic dynamic range relative to the nuclear dynamic range. Compartmentalization is not the entire explanation, however, as rhod-2's nuclear dynamic range is greatly reduced relative to its in vitro dynamic range, and there are no membrane bound organelles inside the nucleus. This reduction of intracellular dynamic ranges, relative to cuvette values, has held true for all fluorescent calcium indicators examined ***(35–37)***. Although the cause of the decrease is not certain, a quenching process associated with the binding of the indicators to intracellular constituents seems likely. What is certain is that the combination of an increased intracellular K_D and a decreased intracellular dynamic range creates in vivo calibration curves that bear little resemblance to the in vitro curves.

3.5. High Spatio-Temporal Resolution Imaging

To this point, the focus has been on the nature of the fluorescent calcium signals rather than confocal microscopy, although the *Z*-resolving power of the confocal, i.e. the ability to resolve signals to specific *Z* depths in the cell (**Fig. 2**), was mentioned. The power of the confocal for calcium imaging is best exemplified, however, by the use of linescans—rapid, 1-dimensional calcium images that have been used with great success in many applications. These include, for example, the imaging of calcium sparks in muscle ***(63)***, calcium waves in starfish oocytes ***(64)***, dendritic and somatic calcium signals in Purkinje cells and thalamic neurons ***(16,60)***, and population activity in behaving zebrafish ***(21,65)***. These linescans have an unparalleled combination of spatial resolution, temporal resolution and signal-to-noise ratio (**Note 24**). This is especially true of linescans acquired via 2-photon imaging, a remarkable tool that has provided insights into intracellular dynamics in stereocilia ***(66)*** and dendritic spines ***(67,68)***. Although two-photon linescans are not technically "confocal," they exhibit remarkable Z-sectioning and are often acquired via a laser-scanning instrument in the same manner as confocal linescans. The beauty of linescans will be illustrated by their usage with two different calcium indicators as we return, for a last time, to the examination of persistent nuclear-cytoplasmic fluorescence gradients.

Figure 8A shows a linescan across a cultured bullfrog neuron loaded with the 70,000 mol wt version of CGD (CGD-70k). These experiments are done using a physiological solution (**Subheading 2.1.2.**) that contains 100 μ*M* of the calcium indicator. Because there is no BAPTA, the indicator also serves as the primary calcium buffer. In this situation the cell controls its resting calcium level, while the indicator acts mainly as a "sensor" of calcium dynamics (but *see* **Note 25**). Depolarizing the cell for 200 ms admits a large bolus of calcium at the edges of this relatively large (50 μm diameter) cell. The spread of calcium across the cytoplasm, into the nucleus and across the nucleolus is clearly visualized. Fluorescence changes in the six specific regions indicated in **Fig. 8A** are plotted in **Fig. 8B**. Calcium rises fastest at the left and right edges of the cell. In the next two regions in from the edge (central cytoplasm; left edge of nucleus), calcium rises more slowly. Although these two inner regions are equidistant from the plasma membrane, calcium rises more slowly in the nucleus, most likely because diffusion into the nucleus is restricted to the small area encompassed by the nuclear pores ***(69)***. The most central regions of the cell rise the slowest. The fluorescence values in **Fig. 8B** have all been normalized to the resting fluorescence in each region, which eliminates indicator concentration as a variable (**Note 26**). The resolution of even the nucleolar signal illustrates the detailed spatial and temporal resolution provided by confocal linescans.

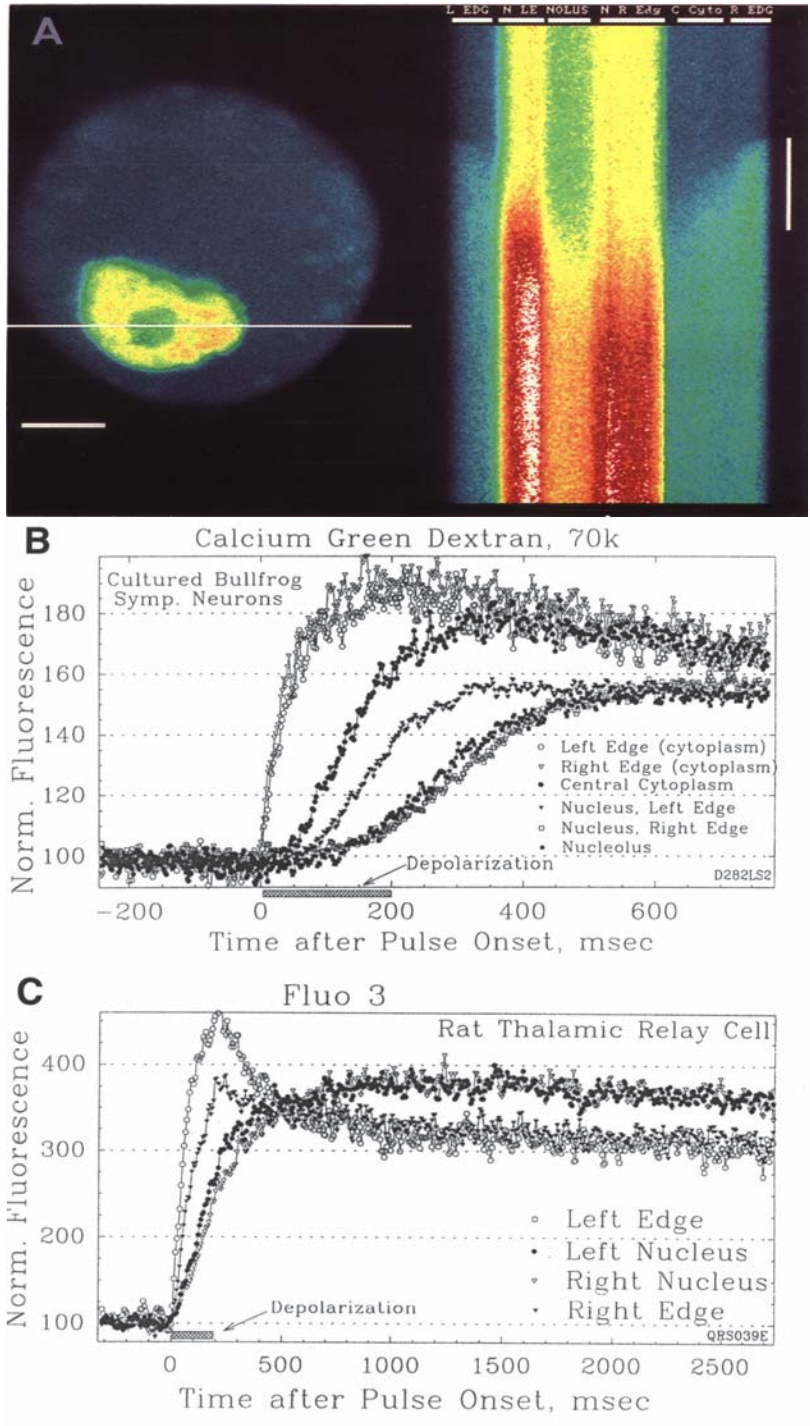
A
L EDG N LE NOLUS N R Edg C Cyto R EDG
B
Calcium Green Dextran, 70k
Cultured Bullfrog
Symp. Neurons
Norm. Fluorescence
180
160
140
120
100
Left Edge (cytoplasm)
Right Edge (cytoplasm)
Central Cytoplasm
Nucleus, Left Edge
Nucleus, Right Edge
Nucleolus
Depolarization
D282LS2
−200
0
200
400
600
Time after Pulse Onset, msec
C
Fluo 3
Rat Thalamic Relay Cell
Norm. Fluorescence
400
300
200
100
Left Edge
Left Nucleus
Right Nucleus
Right Edge
Depolarization
QRS039E
0
500
1000
1500
2000
2500
Time after Pulse Onset, msec

Using this indicator, the relative fluorescence change is higher in the cytoplasm than in the nucleus. Data of this sort have been used to argue that the nucleus is insulated from cytosolic calcium transients ***(70)***. But it is not clear how calcium could, e.g., rapidly rise in the left nuclear region, for about 300 ms, and then abruptly level off even though the adjacent cytoplasm is, by this interpretation, much "higher" in calcium. Even more puzzling is how the deeper nucleoplasmic calcium levels rise for an additional 200 ms, i.e., well after the nuclear pores were ostensibly "shut" at a point about 300 ms into the experiment. The simpler explanation is that these different subcellular regions have independent calibration curves and show different relative fluorescence increases for the same increase in free calcium. Our conclusions are based on the intracellular perfusion and calcium pulsing approach to calibration where we observed free passage of calcium across the nuclear envelope at calcium levels well into the micromolar range. In contrast, Al Mohanna et al. ***(70)*** hypoosmotically shocked cells in distilled water to isolate the nuclei and then calibrated the fluorescence signals from the isolated nuclei. They concluded that the pores are effectively "shut" at cytosolic calcium levels above 300 n*M*.

Fig. 8. *(opposite page)* Nuclear and cytosolic calcium dynamics. **(A)** Fluorescence responses are measured in different regions of a cultured bullfrog sympathetic neuron filled with 100 μ*M* 70K-CGD (and no BAPTA). The indicated line is scanned at 2 ms intervals; successive lines are plotted from top to bottom in the right-hand panel. The cell is depolarized for 200 ms, during the time indicated by the vertical bar. Calcium influx is evident at both edges of the cell beginning from the onset of the depolarization. *See* Color Plate III, following page 372. **(B)** The fluorescence responses in six different regions of this cell, normalized to their respective resting fluorescence levels, are plotted. Calcium is seen diffusing through the cytoplasm, into the nucleus, and across the nucleolus. A clear lag in the nuclear signal is seen by comparing the left edge of the nucleus (N LE) to the central cytoplasm (C Cyto); these regions are equidistant from the plasma membrane. The nucleolus and the right edge of the nucleus rise the slowest. The nuclear regions all show smaller relative fluorescence responses than the cytoplasm, as was also observed in calibration experiments (**Fig. 3**). Only the transient fluorescence gradients are believed to be calcium gradients. The persistent fluorescence gradients most likely reflect the behavior of the indicator. Calcium appears to have largely equilibrated across the cell at about 400 ms after the depolarization. **(C)** In a similar type of experiment, but now using a slice from rat brain, a thalamic neuron is loaded with 100 μ*M* fluo-3. It shows fluorescence responses in the nucleus that are larger than those in the cytosol. This agrees with our results using fluo-3 in cultured neurons. The rapid flux of calcium across the nuclear envelope again suggests free communication (for small molecules) between nucleus and cytoplasm. (**Figure 8C** is courtesy of Dr. Qiang Zhou, Dept. of Pharmacology, UCSF, San Francisco, CA.)

Given the many and drastic ways that fluorescent calcium indicators are influenced by the intracellular environment, exposing nuclei to distilled water seems unlikely to provide a physiologically relevant calibration.

In contrast to the CGD results, with fluo-3-loaded bullfrog sympathetic neurons, the nuclear fluorescence responses are larger than the cytoplasmic responses. This is observed in other types of neurons including, e.g., thalamic relay cells in slices of rat brain (**Fig. 8C**). In this experiment, a relay cell was depolarized for 200 ms producing a rapid calcium increase at the edges of the cell. The two nuclear regions rise more slowly, but reach a higher plateau than the cytosolic regions. Data of this sort, including early data from our laboratory, have been widely interpreted to mean that the nucleus amplifies the cytosolic calcium signal ***(19,62,71)***. This observation could alternatively be explained by compartmentalization of a small fraction of the cytoplasmic fluo-3 into calcium-containing organelles, as mentioned earlier, or by other differences in the nuclear and cytoplasmic environments. What is especially difficult for the proponents of persistent nuclear/cytosolic calcium gradients to explain is how the nucleus can insulate itself from cytoplasmic calcium gradients when loaded with calcium green dextran, but then generate amplified nuclear signals when loaded with fluo-3. As unlikely as this may seem, there are many active proponents of the idea that the nucleus actively regulates its free calcium levels ***(72–76)*** and so the mechanistic implications of the "persistent calcium gradient" interpretation should be discussed.

The nuclear envelope is actually a double membrane structure that forms a compartment (the lumen of the nuclear envelope) surrounding the nucleus. Thus, calcium ATPases in the outer membrane of the nuclear envelope will pump calcium into the lumen but would not pump calcium into the nucleus proper. The only structure that spans both the inner and outer membranes of the nuclear envelope are the nuclear pores. These pores are believed by most biologists to universally pass small molecules (**Note 27**). It is not clear how a gradient of free calcium could be created or maintained across the nuclear envelope given such cell biological data. In fact, if one believes both the amplification and the insulation theories, one must propose two sets of mechanisms—one pumping calcium across two membranes into the nucleus, the other pumping calcium across two membranes out of the nucleus. Our dynamic imaging data do not fit with this. Our observations show calcium rushing into the nucleus in every calcium imaging experiment we've done—including every indicator tested, every neuronal cell type studied, and in every preparation ranging from cultured bullfrog sympathetic neurons, to thalamic cells in rat brain slices, to hindbrain neurons in living zebrafish. It seems much simpler to attribute the fluorescence gradients to the known "eccentricities" of the various indicators (and to the vagaries of the loading mechanisms) rather than to a

new and fantastic set of molecular machinery whose existence is based solely on persistent fluorescence gradients.

In spite of the foregoing arguments, it has not been "proven" that these persistent fluorescence gradients are *not* calcium gradients. This uncertainty reflects the core difficulty of the calibration problem: the difficulty in attaining absolute control over calcium in different subcellular regions while maintaining physiological conditions. This difficulty is at the center of our uncertainties about resting free calcium levels and the absolute size of physiological calcium signals. These limitations notwithstanding, it is clear that confocal calcium imaging provides excellent dynamic information about the location of calcium signals and the size of the fluorescence signals at different locations inside the cell. Indeed, it is the rapid dynamics of the fluorescence signals that gives us the best information about where calcium is changing and by how much. As optical methods continue to improve, and as indicators expand to chloride, sodium and more complex signaling molecules such as calmodulin, cAMP and gene products, confocal activity imaging should advance many areas of cellular and neurobiology. Such advances would be facilitated by vigorous efforts to better understand and judiciously interpret subcellular fluorescence gradients.

4. Notes

1. When fluorescent calcium indicators are loaded directly into the cytosol (via injection or patch-clamping) the nucleus is invariably brighter than the cytosol. This has held true for all cell types and calcium indicators examined, including the ratiometric indicators fura-2 and indo-1. In contrast, in AM-loaded cells, the nucleus is often darker than the cytosol ***(62,77,78)***, consistent with partitioning of an appreciable amount of indicator into either lipid bilayers or cytoplasmic organelles. These dark nuclei are "artifactual" in the sense that they do not reflect selective loading of indicator into the aqueous space of the cell (i.e., cytosol and nucleoplasm). This was confirmed by first loading cells with fluo-3 AM (which yielded dark nuclei) and subsequently perfusing the cells with the salt form of fluo-3 which then produced a bright nucleus. The aqueous labeling was much more responsive to calcium influx than the AM-loaded indicator (Fig. 8 in **ref. *20***). In other cases, AM loaded cells may show a less dark, equifluorescent or even a slightly bright nucleus, most likely reflecting varying degrees of compartmentalization of the indicator. This will cause varying degrees of nuclear/cytoplasmic fluorescence gradients (or ratio gradients) and absolutely precludes directly equating resting image gradients to resting calcium gradients ***(20,26)***. In addition, the subcellular calibration of calcium responses in AM-loaded cells will vary directly with the degree of compartmentalized indicator in each region. This seriously limits the utility of AM indicators in making absolute calcium determinations at different subcellular locations.

2. Although confocal imaging with the two main ratiometric indicators, fura-2 and indo-1, can be done with a UV laser ***(79)***, confocal optics are not usually optimized for passing shorter wavelengths. Also, UV light is generally more harmful than visible light ***(53,80)***. Because photodamage is a major concern in physiological experiments, our preference is to use visible wavelength indicators. There are several possibilities for visible-wavelength ratio imaging. One is to use a mixture of fura red and fluo-3 ***(81)***, which has been used to demonstrate a rapid equilibration of calcium across the nuclear envelope in hamster oocytes ***(53)***. Another potential option is a calcium green–Texas red dextran (CGTRD) conjugate. However, the batch of CGTRD purchased by us showed only a threefold in vitro dynamic range in the calcium green (fluorescein) channel, vs the 10- to 15-fold dynamic range that pure calcium-green dextran provides (other investigators have apparently experienced similar problems). We also attempted using a simple mixture of calcium green dextran and texas-red dextran, but found that Texas red dextran had a much faster bleach rate than the calcium green, which eliminated its utility for ratio imaging. In the fura red/fluo-3 study, the authors did not comment on the number of imaging trials over which the fura red/fluo-3 ratio was stable, but they did report better signal-to-noise ratio and less phototoxicity than with UV-ratio indicators ***(53)***. A third option is to use two-photon (long-wavelength) excitation of a shorter wavelength ratio indicator, since this circumvents UV-induced photodamage. A pilot experiment that we performed in collaboration with the Webb group, using indo-1, suggests that this approach may be useful (*see* Fig. 8 in **ref. *82***).

   The fluorescent calcium indicators discussed in this paper were all purchased from Molecular Probes in Eugene, Oregon. Although some indicators may not have been as successful as hoped, it should be emphasized that all of the imaging work published from our laboratory (and many others) has relied exclusively on these indicators.
3. Our intracellular solution is specifically designed for recording calcium currents. Although a more "natural" intracellular solution would contain KCl, our solution contains cesium gluconate because gluconate is a slightly better anion than chloride for general preservation of the cell and because cesium reduces potassium currents that would interfere with our recordings of calcium currents. The compound tetraethylammonium (TEA) is also used to block potassium currents. The extracellular solution is a standard Ringer's, but contains tetrodotoxin (1 μ*M*) to block sodium currents (*see* **ref. *20*** for more details). This simple formula allows the recording of robust calcium currents in cultured bullfrog sympathetic neurons. More complex formulae, e.g., containing an ATP-regenerating system, can be used ***(16)***. A formulary providing many helpful details on the makeup of intracellular solutions is available ***(83)***.
4. One calcium calculation program, called MAXC, is available via the internet at http://www-leland.stanford.edu/~cpatton, and was written by Chris Patton at the Hopkins Marine Station in Pacific Grove, CA. Bers et al. ***(31)*** discuss the use of this program which is currently available for IBM/Windows operating systems.

This program might be run on MacIntosh systems using "Virtual PC" (Connectix, San Mateo, CA). Our laboratory uses a similar type of program written by Alvaro Villaroel in the ASYST electrophysiological programming language.

5. For our experimental conditions, BAPTA's K_D would be about 210 n*M*, using the values of Harrison and Bers ***(84)***. However, taking the original value of Tsien ***(30)*** and correcting it for osmolarity based on Harrison and Bers' results yielded a K_D of 160 n*M* at 23°C. This latter K_D provided a somewhat better fit between our observed and predicted fluorescence for fluo-3 and has been used for all calcium calculations in this chapter. A variety of factors should be taken into account in preparing calcium standards and calcium buffer solutions, including, e.g., purity of the buffer. These have been discussed in detail ***(31,85)***.

   It may seem problematic that the makeup of the calibration solutions is based, in part, on the K_D of the indicator, which is the unknown being determined. However, because there is a 100-fold greater concentration of BAPTA (10 m*M*) than indicator (100 μ*M*), the error that results from uncertainty in the indicator's in vitro K_D is negligible. For example, increasing fluo-3's K_D from 400 n*M* to 800 n*M* would increase the free calcium in the "100 n*M* solution" to only 100.4 n*M*.
6. Calcium-sensitive electrodes are an alternate technique for measuring free calcium levels, but the most commonly available electrodes are not very accurate at low calcium levels, i.e., in the 50 n*M* to 300 n*M* range, where much calcium activity of interest occurs. A more sensitive calcium electrode has been developed, but its use and characterization have thus far been limited ***(86)***.
7. A square coverslip is glued onto the bottom of a 35-mm Petri dish with General Electric RTV 615A adhesive (aquarium sealant has also been used). These chambers or "confocal cuvettes" are cleaned before each experiment. After they are cleaned and rinsed with distilled water, the excess water is shaken off and any remaining droplets of water in the chamber are removed by puffs of air from a pipette bulb fitted with a short plastic tube. This avoids residues left by Kim wipes or spray cleaners. We use either a conventional cove slip (no. 1–1/2) for cell culture or droplet-calibration studies, or a thinner cover slip (no. 1) when looking deeper into tissue, e.g., when looking 200 μm into the larval zebrafish hindbrain.

   This "confocal cuvette" may be thought of as a virtual cuvette in the sense that it is delineated in the Z-dimension by the optical section thickness (principally a function of the microscope objective lens) and in the XY-dimension by the measuring box (a standard feature of confocal software) used to quantitate the fluorescence. With appropriate solution filtering and chamber cleaning, these droplets are fairly uniform in fluorescence when the "confocal cuvette" is fully enclosed in the droplet, i.e., positioned just high enough above the coverslip to obtain a maximal signal.
8. Obtaining reproducible, quantitative fluorescence measurements requires careful attention to the confocal instrument's settings: aperture, gain, neutral density filtering, black level, and acquisition mode (e.g., we use the "low signal" setting on the Bio-Rad MRC 600). Because our experiments are conducted in this mode,

we've constructed our calibration curves using this setting. With our settings, we find that turning the "autoblack" function off and manually setting the black level provides the most stable frame-to-frame baseline within imaging trials (such trials typically last about 1–10 s). However, turning off the autoblack function also reveals a slow but substantial drift in black level, especially while the scan box is warming up. We allow the scan box to warm up for 2 h or more prior to imaging. Thereafter, the black level shows modest slow fluctuations; it is periodically checked and adjusted as needed.

Ideally, all fluorescence measurements would be taken at the same instrument settings. However, with the 256 unit gray scale of the MRC 600 and the low signal setting, we found that the most linear fluorescence measurements were taken with average pixel intensities between about 30 and 200. With this limited range, it was not possible to record the fluorescence values of all calcium levels at a single photomultiplier (PMT) gain setting. Thus, it was necessary to decrease the gain when higher calcium concentrations were measured. By measuring test droplets and test slides at different gain settings, correction factors were generated and used to scale all the fluorescence measurements to a common scale ***(20)***. Newer confocals with expanded (12-bit) gray scales may not require this, but the fluorescence linearities of all confocals should be checked under the settings used in the conduct of the calcium imaging experiments. Commercial fluorescence standards and serial dilution of fluorescent solutions can be used for this purpose.

9. Ratiometric calcium imaging is often believed to solve the "calibration" problem because it factors out indicator concentration and because a given ratio can, in theory, be directly equated to a free calcium concentration. In practice, the problem of intracellular alteration of indicator behavior is so great that ratio imaging has not resolved the conflict over resting free calcium in muscle cells, where this issue has been most intensively studied. Factors that alter the behavior of ratio indicators include spectral shifts caused by binding or compartmentalization of the indicator—processes that can vary over time and from cell to cell ***(34,39–42)***. Other factors include changes in ratio with photobleaching (possibly oxidation) and, conversely, ratio changes with de-oxygenation, a technique that might be used to prevent photobleaching ***(87–89)***. These indicators also show changes in calcium/magnesium selectivity ***(90)*** and, in the case of brain slices, changes in ratio with increasing depth in the slice (A. Konnerth, personal communication). These factors limit the accuracy with which the ratio method can establish the level of resting free calcium. Indeed, a set of calcium images documenting the subcellular, in vivo behavior of fura-2 or indo-1 across a range of known calcium levels remains to be published. If several ratio imaging studies can come to a consensus that a particular subcellular ratio of indo-1 or fura-2 represents a specific level of free calcium, then that would bolster the utility of ratio imaging for obtaining absolute calcium levels.
10. Electrophysiological techniques are described in several books ***(91–93)*** including a technical manual from Axon Instruments called The Axon Guide ***(94)***. Standard patch-clamp techniques are used for these experiments, but nonelec-

trophysiologists would be best served by seeking an instructor or course to learn this skill. Our confocal configuration allows an electrophysiological recording station to sit beside the vibration isolation table that holds the confocal microscope. This minimizes the time required to set up an electrophysiological experiment. For our experiments, set up mainly involves placing the preparation on the stage of the inverted microscope, connecting the flow lines and attaching an electrode holder to a micromanipulator mounted on the stage. The bullfrog neurons are cultured on the cover-glass bottomed wells made from plastic Petri dishes (**Note 7**). These dishes are secured to a standard microscope stage (that accepts 35-mm Petri dishes) and connected to the inflow and outflow lines. The patch electrode is then inserted into its holder and positioned near the cell. The patch electrode is moved to within about 5 µm of the cell using a 20X objective lens, but the final seal is made only after switching to the 50X Leitz (water immersion, 1.0 NA). The 50X Leitz provides a very bright signal relative to many other objectives that we've tested. A newer 40X/0.75 Zeiss achroplan (infinity-corrected) lens was recently found to have comparable performance to the 50X Leitz, even though it is not coverslip corrected. Experiments on brain slices are more complicated and require use of an upright microscope as described in Zhou et al. ***(16)***. In such experiments, the laser beam is redirected via a pair of mirrors to a Zeiss standard 16 upright microscope that is placed next to the inverted microscope. The slices are then imaged with a Zeiss 40X/0.75 dip lens. For studies on cultured cells, a minimum of one uninterrupted day per week of confocal time seems necessary to make even modest experimental progress; two or more contiguous days is desirable for brain slice or intracellular perfusion experiments.

11. For large bullfrog neurons (typically about 50 µm in diameter), the indicator fluorescence inside the cell did not reach a plateau even after 15–20 min of filling, although the rate of fluorescence increase slowed markedly by this point. This gradual fluorescence increase could be due to a variety of factors, including (1) slow binding or gradual compartmentalization, (2) depletion of indicator from the tip of the patch-electrode, (3) gradually rising calcium levels, (4) increased access resistance through the patch electrode, or (5) some combination of the above. However, after the initial rapid filling phase is complete, the minute-to-minute changes in fluorescence are quite modest in comparison to the rates of calcium increase produced by the experimental manipulations (calcium pulses and intracellular perfusion).
12. A detailed description of the intracellular perfusion technique is provided by Yu et al. ***(18)*** and Lopez ***(95)***. Because the available time on a confocal microscope is usually limited, and because the setup and execution of intracellular perfusion experiments are somewhat intricate, this type of calibration is not easy. Proficiency at patch-clamping is essential. A useful approach is to first gain skill in intracellular perfusion on a nonimaging electrophysiology station, by e.g., changing the concentration of sodium in the patch pipet so as to reverse the cell's sodium gradient ***(18,96)***.

The patch-clamp electrode is pulled with a very short shank to allow the closest possible apposition of the internal (perfusion) tube to the tip of the electrode. These electrodes are typically made to have a low resistance, about 1–4 megaohms. Colored solutions are helpful in working out the flow performance of the perfusion system. The "back end" of the inflow line rests in a small (typically 1 mL) reservoir or vial containing Solution B. The "front end" of this line is threaded though the O-ring seal in the electrode holder and connected to the quartz internal perfusion tube. The outflow line runs from a side port on the electrode holder to a small rubber-stoppered bottle, and is connected to one of two metal tubes inserted through the top of the bottle. A second line, connected to the second metal tube, runs from the outflow bottle to the electrophysiologist and is used to make the initial patch-clamp seal. By applying suction to and then clamping this second line, sufficient vacuum is created to pull solution B through the inflow line (after its valve is opened) and into the pipet tip. Solution A is simultaneously pulled through the outflow line and drops into the small outflow bottle. All solutions are carefully filtered with a 0.2 μm nylon filter; this is critical to prevent blockage of the small inflow tube inside the patch-clamp pipet.

13. Because binding of calcium to indicators is a hyperbolic process, indicators are not completely saturated even at very high calcium levels. However, attaining calcium levels reasonably near saturation, e.g., 95–97% saturated, is usually sufficient to provide an adequate description of the indicator's K_D and dynamic range—especially in the context of the other uncertainties faced. For example, whereas 99% saturation of fluo-3 in our calibration solution requires 39 μ*M* free calcium, 97% requires only 13 μ*M* and 95% saturation just 7.6 μ*M*. For our purposes, 95% saturation would be acceptable because it would mean that we have 95% of the maximum dynamic range of the indicator. Given that free calcium in the pipet (when filled with high-calcium solution) is in excess of 100 μ*M*, it seems likely that the cytoplasmic indicator is at least 95% saturated. By increasing total calcium to 12 m*M* (vs the 10 m*M* BAPTA in the solution), far higher (and more toxic) concentrations of free calcium can be employed.
14. That nuclear fluorescence exceeds cytosolic fluorescence is true for many fluorescent dyes such as Lucifer Yellow and for all non-AM fluorescent calcium indicators tested, including ratiometric indicators such as fura-2 and indo-1. Consideration of the alternative hypothesis, however, is instructive. Were the resting fluorescence gradient due entirely to a resting calcium gradient, than the large parallel increases during intracellular perfusion would mean that the nucleus is somehow able to sample cytosolic free calcium and, for every sized increase in cytosolic calcium, produce an increased but proportionately sized calcium response in the nucleus by a mechanism that spans the outer nuclear membrane, the lumen of the nuclear envelope, and the inner nuclear membrane. Such a remarkable mechanism would certainly be interesting. It is far simpler, however, to attribute the fluorescent gradient to the well-known binding of indicators to intracellular constituents or to the exclusion of highly charged indicators from cytoplasmic organelles, or perhaps, to some combination of these and other factors.

15. The "far from saturation" argument cannot explain the nuclear fluorescence increase if the resting fluorescence gradient is attributed to a calcium gradient. In these early experiments (using CsCl-based solutions) the cell was filled not with 0 calcium solution, but with a very low calcium solution (10 n*M*) to better preserve the health of the cell (this was not necessary in later experiments where cesium gluconate was used). A 10 n*M* free calcium concentration actually "uses up" a portion of the in vitro dynamic range, reducing the remaining available dynamic range to no more than about 35-fold. With this starting condition, if nuclear calcium were at twice the cytosolic calcium level, i.e., at 20 n*M*, than its observed 24-fold increase would not be possible. Even if one argues that only part of the resting fluorescence gradient is a calcium gradient (with the remainder being an indicator fluorescence gradient), the argument still encounters problems. Because the nuclear fluorescence begins "higher" on the calibration curve, it will begin to approach diminished fluorescence returns before the cytosolic calcium signal does. It should therefore show a smaller fluorescence increase than the cytosol. In fact, it does exactly the opposite—it increases 24-fold vs. the cytosol's 18-fold increase (Fig. 7 in **ref. *20***). This difference is most easily explained by a gradual internalization of a small amount of fluo-3 into cytoplasmic organelles, i.e., into a compartment where it is already resting at higher than cytosolic calcium levels and is therefore less sensitive to cytosolic calcium increases. This would thus diminish the cytoplasmic fluorescence increase relative to the nuclear increase (where none of the indicator is shielded inside membrane bound organelles). Another line of evidence in favor of this idea is the fall in the nuclear/cytoplasmic ratio when cells are initially filled with indicator (this was true for all calcium levels tested; *see* Fig. 5 in **ref. *20***). At the outset of filling there would be no compartmentalized fluo-3 (it has a -5 charge), but if it very gradually enters mitochondria, the endoplasmic reticulum (ER) or other compartments, it will selectively increase the cytoplasmic signal (especially if it is entering compartments that are high in calcium), thereby causing the nuclear/cytoplasmic ratio to fall.
16. Voltage clamp is described in *The Axon Guide* ***(94)*** and in Johnston and Wu ***(93)***, and involves injection of current (either positive or negative) to hold the cell at a specified voltage. From the holding potential, depolarizing voltage steps or pulses are used to administer calcium to the cell. From a membrane potential of –70 mV, depolarization to 0 mV maximally activates calcium currents in these cells. To flood cells with calcium, 70 ms long voltage pulses are given at 5 Hz until the cell's fluorescence reaches a steady plateau. This typically requires only a few tens of seconds or less.
17. Initially, the peak efflux rate may be quite substantial, as suggested by an initially rapid fall in dendritic calcium signals observed in thalamic relay cells (Fig. 3 in **ref. *16***). However, this falling phase involves not only efflux but also uptake of calcium into internal stores which have a limited capacity. In addition, the Na^+/Ca^{2+} exchanger's removal of calcium depends on the influx of sodium down its concentration gradient which may also be limited by a build up of sodium near

the plasma membrane during the large influx of calcium produced by repetitive voltage pulses ***(2,48)***.

18. The K_D of an indicator is determined based on the maximum fluorescence increase it exhibits when starting from a given free calcium level. First, a normalized "starting fluorescence," *F*, is determined using the equation $F = (8.65/FI) \cdot 100$, where 8.65 was CGD's total dynamic range during this series of experiments and *F*I = the observed fluorescence increase (final fluorescence/pre-stimulation fluorescence). The percentage of indicator with bound calcium, *B*, is then directly calculated by entering *F* into the equation: $B = (F - 100)/7.65$. This value for *B* is the "observed" value for the percentage of indicator bound and is equal to the amount of indicator bound, in μ*M*, as we use 100 μ*M* total indicator. The calculation program is then entered with the starting free calcium level and the total concentration of calcium green dextran (100 μ*M*) and is then used to obtain a "calculated" value for *B*. The K_D of calcium green dextran is now varied by trial and error until the calculated value for *B* is equal to the observed value for *B*—this is the intracellular K_D. Although this may not be the simplest approach for determining the intracellular K_D, it provides independent K_D's for each starting calcium level and is quite practical when using our calculation program.
19. There is obviously substantial variability in our determinations of CGD's intracellular K_D. Although this is far from ideal, we are not aware of any calcium imaging study where intracellular K_D determinations have been made from a range of different starting calcium levels. More work in this area is clearly needed. If nothing else, this determination provides, at a minimum, a check on the indicator's intracellular behavior and a sense of the reliability of the K_D used in one's calculations.
20. It may seem odd to assume a level for resting free calcium given the focus of this chapter on real calibrations. However, the absolute level of resting calcium remains controversial for muscle cells and even more uncertain for other cell types. Although ratio imaging might seem to ameliorate this problem, there are serious limitations to determining absolute calcium levels even with ratiometric indicators (**Note 9**). Regarding a ratiometric study reporting widely varying resting calcium levels among different cells in a population ***(97)***, it seems that variability in compartmentalization of the indicator is at least as tenable an explanation for the different resting ratios as variability in resting calcium (perhaps even more tenable because the calcium pumps that set resting calcium would be expected to be identical from cell to cell). Until the issue of resting calcium is resolved, it seems that assuming a resting free calcium level (and testing the effects of this assumption) is as satisfactory as other methods for estimating the magnitude of intracellular calcium signals.
21. **Equation 2** can be used to construct the curves in two ways. The simplest is to just insert a range of *F* values into the equation and directly calculate free calcium. Alternatively, one can start with a range of calcium concentrations and solve for *F*. This is essentially what the iterative calculation programs do, although our program actually yields the amount of indicator-bound calcium from

which we calculate the fluorescence, F, using the CGD version of **Eq. 1**: $F = (100 - B) + 8.7B$, where B = % of indicator bound to calcium. If one is lacking a calculation program, it is also possible to choose a free calcium level and solve **Eq. 2** for F by trial and error.

22. The crux of the problem was that the somatic high-threshold (HT) calcium channel response was substantially larger than the somatic LT calcium channel response. Responses for both channel types increased from the soma to the dendrites, but the relative increase for the low-threshold channels was greater than for the HT channels (Fig. 3 in **ref. *16***). When 100 n*M* resting calcium was assumed, the dendritic fluorescence response of the HT channels, even though proportionately smaller than the LT response, pushed the HT response into the near-plateau region of the fluorescence vs calcium curve, creating a calcium increase that was proportionately larger than the LT calcium response. In contrast, with the 50 n*M* resting calcium assumption, the responses were in a more linear region of the curve and the relatively larger fluorescence increase observed with the LT channels would be consistent with the LT calcium signals having increased more from soma to dendrites than did the HT calcium signals.
23. A possible misconception is that calcium buffering might account for persistent calcium gradients, such as the proposed nucleolar/nucleoplasmic gradient. Although buffer concentration shapes the dynamics of calcium transients and affects the magnitude of the increase in free calcium produced by a bolus of calcium ***(98,99)***, it does not set steady-state levels of calcium. The resting level of free calcium (and therefore the gradient across the cell's membranes) is set and maintained actively by pumps and exchangers in the plasma membrane and organellar membranes. It is only by expenditure of energy that a persistent nucleolar/nucleoplasmic calcium gradient could, in theory, be generated. Because there are no pumps or exchangers at the nucleolar border, and no membrane at the nucleolar border to maintain any gradient that was generated, it is difficult to imagine how this persistent fluorescence gradient could be due to a calcium gradient. When a "finding," such as this, seems to violate physical laws, such as the first and second laws of thermodynamics, one should carefully scrutinize the underlying assumptions— in this case the assumption that the indicator is behaving the same in different nuclear regions.

    Another observation of nucleolar calcium signals raises further problems for subcellular calibration. In cells filled with fluo-3 or calcium green dextran, the nucleoli are typically dimmer than (or equifluorescent with) the nucleus proper (see **Fig. 2A** and **Fig. 8**). However, when cultured neurons were in declining health, the nucleoli of fluo-3-loaded cells usually became brighter than the nucleus proper, as shown in **Fig. 2B**, where an XZ scan of a cell at the end of an experiment showed a prominent nucleolus. Although this cell looked fine morphologically, its input resistance had declined significantly indicating possible damage to the plasma membrane. In every fluo-3-loaded cell that showed nucleolar changes, the pattern was always one of dark nucleoli becoming bright (relative to the nucleus), indicating a change in state of the nucleolus that affected the

binding or fluorescence of fluo-3. A more deliberate means of inducing an irreversible subcellular fluorescence gradient is to repetitively scan a single line at a higher laser intensity. This rapidly induces a permanent increase in the fluorescence of that line (see Fig. 3 in **ref. *100***). Such permanent alterations in fluorescence obviously pose considerable problems to calibration efforts, and should be considered if unusual fluorescence gradients are encountered.

24. Single lines can be scanned at 2 ms intervals on the Bio-Rad MRC 600 and even faster on newer confocal microscopes. Although these images are spatially "one-dimensional," they provide detailed information about calcium dynamics at different locations either within a cell or across multiple cells. The information sought in a "two-dimensional" image can, in many cases, be acquired by placing a scan line across the regions of interest. Although the MRC 600 provides only horizontal linescans, some newer confocal imaging systems allow the scan line to be oriented in any direction. One caution is that such off-axis (nonhorizontal) linescans may not be truly linear, but can be slightly elliptical, thereby skirting a target if the target is small. The fidelity of the oblique linescan can be checked by allowing a fluorescent solution to evaporate in a glass-bottomed Petri dish, creating a thin film of dye. Repetitively scanning a line at one specific orientation will then bleach the film and allow the fidelity of the linescan to be evaluated (E. Lumpkin, personal communication). Although the rate for acquiring two-dimensional images is becoming faster, the pixel dwell time must be drastically reduced in order to achieve the same scan rate as a linescan. It is not clear that a signal to noise ratio comparable to that of linescans can be achieved with such short pixel dwell times.
25. This is not strictly true—buffering of calcium by fluorescent indicators can alter the "shape" of cellular calcium signals, including the rate that calcium diffuses across the cell and the height of calcium transients ***(59,98,99)***. The exact manner in which indicators perturb the "normal" calcium transient depends on their K_D, concentration and molecular weight. Whereas small molecular weight indicators might collapse or dissipate gradients ***(98)***, large molecular weight indicators, such as the 70K dextran used in **Fig. 8A**, may act as a barrier, slowing the diffusion of calcium across the cell. The effect of indicator concentration depends on the extent to which it overwhelms the endogenous buffering capacity of the cell. Endogenous buffers, including both calcium binding proteins and negatively charged phospholipids, are thought to constitute a total buffering capacity in the range of 50–500 μ*M* ***(101–103)***, with some classes of neuron having large amounts of specific calcium binding proteins ***(3,104)***. Our use of a 100 μ*M* concentration of indicator might, therefore, constitute a considerable fraction of total cellular buffering and would change the shape and time course of calcium dynamics. Nonetheless, we found that the pattern of calcium influx is similar at both 100 μ*M* and 20 μ*M* fluo-3 (unpublished observations). The lower concentration would be expected to have only minimal effects on the native transients, so we expect that, in general, our experiments reflect fairly accurately the pattern of influx, which is important for such issues as localization of calcium channels

subtypes. Lower indicator concentrations would be expected to require more intense laser illumination, thereby increasing phototoxicity. However, use of 10 μ*M* indicator has recently been reported to not only yield larger relative fluorescence responses, but also, to produce a more stable, long-lasting signal (Kovalchuk and Konnerth, pers. comm.). At the opposite end of the spectrum, in cells loaded with 10 mM BAPTA and 100 μ*M* fluo-3, the BAPTA completely suppressed the fluorescence transients that would normally have occurred after a long calcium pulse (200 ms or more; *see*, e.g., Fig. 5b in **ref. *20***). Thus the buffering capacity of the indicators, while not problematic for some questions, should be considered in cases where the precise time-course and absolute magnitude of the subcellular calcium transients are essential to interpretation of the experiment.

26. As noted previously, ratiometric imaging eliminates indicator concentration as a variable. The analysis used in **Fig. 8B** and **Fig. 8C**, taking a ratio of the evoked fluorescence increase over the resting fluorescence, is analogous to ratiometric imaging in that indicator concentration is again factored out of the equation. As such, this approach should (as a first approximation) give the relative calcium changes in different subcellular regions. This assumes, however, that free calcium is uniform across the cell at rest. This seems likely to be the case in the soma, at least, because calcium can equilibrate across the cell fairly quickly (dendrites and axons are a separate matter). But if the resting fluorescence gradients represented resting calcium gradients, then this approach provides less information. The higher resting nuclear fluorescence observed is not unique to single wavelength indicators, because the main ratiometric indicators, indo-1 and fura-2, also show a bright nucleus at both wavelengths used for the ratio imaging.
27. In every study where molecules such as fluorescent dextrans have been injected into the cytosol, they have been shown to freely enter the nucleus (almost certainly via the nuclear pores) so long as their molecular weight was 20,000 or less ***(105,106)***. Indeed, in our cells, even the 70,000 M_r CGD entered the nucleus almost immediately after formation of a whole-cell patch-clamp recording. Although compounds of molecular weights over 70,000 (up to 500,000) traverse the pores by an active mechanism that can be regulated, there is a large body of data showing that compounds under 20,000 are never prevented from diffusing into or out of the nucleus ***(107)***. Given this physical situation, it is difficult to imagine how the nuclear pores can be completely open to calcium one instant, and then closed to calcium the next instant, which would seem necessary if one is to interpret the persistent fluorescence gradients in **Fig. 8** as persistent "calcium" gradients. If one does not argue for complete closure of the pores, then one must construct an elaborate transenvelope pumping system that would maintain the gradients (and in fact create the gradient for the amplification scheme).

References

1. Krause, K. H. (1991) Calcium-storage organelles. *FEBS Lett* **285,** 225–229.
2. White, R. J. and Reynolds, I. J. (1995) Mitochondria and Na^+/Ca^{2+} exchange

buffer glutamate-induced calcium loads in cultured cortical neurons. *J. Neurosci.* **15,** 1318–1328.

3. Baimbridge, K. G., Celio, M. R., and Rogers, J. H. (1992) Calcium-binding proteins in the nervous system. Trends Neurosci. 15, 303–308.
4. Takei, K., Stukenbrok, H., Metcalf, A., Mignery, G. A., Sudhof, T. C., Volpe, P., and De Camilli, P. (1992) Ca^{2+} stores in purkinje neurons, endoplasmic reticulum subcompartments demonstrated by the heterogenous distribution of the $InsP_3$ receptor, Ca^{2+}-ATPase, and calsequestrin. *J. Neurosci.* **12,** 489–505.
5. Andressen, C., Blumcke, I., and Celio, M. R. (1993) Calcium binding proteins, selective markers of nerve cells. *Cell Tiss. Res.* **271,** 181–208.
6. Pozzan, T., Rizzuto, R., Volpe, P., and Meldolesi, J. (1994) Molecular and cellular physiology of intracellular calcium stores. *Physiol. Rev.* **74,** 595–630.
7. Miller, R. J. (1988) Calcium signaling in neurons. *Trends Neurosci.* **11,** 415–419.
8. Gnegy, M. E. (1993) Calmodulin in neurotransmitter and hormone action. *Annu. Rev. Pharmacol. Toxicol.* **32,** 45–70.
9. Kasai, H. and Petersen, O. H. (1994) Spatial dynamics of second messengers, IP3 and cAMP as long-range and associative messengers. *Trends Neurosci.* **17,** 95–101.
10. Ghosh, A. and Greenberg, M. E. (1995) Calcium signaling in neurons, molecular mechanisms and cellular consequences. *Science* **268,** 239–247.
11. Baylor, S. M. and Hollingworth, S. (1988) Fura-2 calcium transients in frog skeletal muscle fibres. *J. Physiol.* **403,** 151–192.
12. Llinas, R., Sugimori, M., and Silver, R. B. (1995) The concept of calcium concentration microdomains in synaptic transmission. *Neuropharm.* **34,** 1443–1451.
13. Robinson, I. M., Finnegan, J. M., Monck, J. R., Wightman, R. M., and Fernandez, J. M. (1995) Colocalization of calcium entry and exocytotic release sites in adrenal chromaffin cells. *Proc. Natl. Acad. Sci.* **92,** 2474–2478.
14. Grynkiewicz, G., Poenie, M., and Tsien, R. Y. (1985) A new generation of calcium indicators with greatly improved fluorescence properties. *J. Biol. Chem.* **260,** 3440–3450.
15. Tsien, R. Y. (1989) Fluorescent probes of cell signaling. *Ann. Rev. Neurosci.* **12,** 227–253.
16. Zhou, Q., Godwin, D. W., O'Malley, D. M., and Adams, P. R. (1997) Visualization of calcium influx through channels that shape the burst and tonic firing modes of thalamic neurons. *J. Neurophys.* **77,** 2816–2825.
17. Marrion, N. V. and Adams,P. R. (1992) Release of intracellular calcium and modulation of membrane currents by caffeine in bull-frog sympathetic neurones. *J. Physiol.* **445,** 515–535.
18. Yu, S. P., O'Malley, D. M., and Adams, P. R. (1994) M-current regulation by intracellular calcium in bullfrog sympathetic neurons. *J. Neurosci.* **14,** 3487–3499.
19. Hernandez-Cruz, A., Sala, F., and Adams, P. R. (1990) Subcellular calcium transients visualized by confocal microscopy in a voltage-clamped vertebrate neuron. *Science* **247,** 858–862.

20. O'Malley, D. M. (1994) Calcium permeability of the neuronal nuclear envelope, evaluation using confocal volumes and intracellular perfusion. *J. Neurosci.* **14,** 5741–5758.
21. O'Malley, D. M., Kao, Y.-H., and Fetcho, J. R. (1996) Imaging the functional organization of zebrafish hindbrain segments. *Neuron* **17,** 1145–1155.
22. Westerblad, H. and Allen, D. G. (1994) Methods for calibration of fluorescent calcium indicators in skeletal muscle fibers. *Biophys. J.* **66,** 926,927.
23. Baylor, S. M., Harkins, A. B., and Kurebayashi, N. (1994) Response to Westerblad and Allen. *Biophys. J.* **66,** 927,928.
24. Almers, W. and Neher, E. (1985) The calcium signal from fura-2 loaded mast cells depends strongly on the method of dye-loading. *FEBS Lett.* **192,** 13–18.
25. Glennon, M. C., Bird, G. S. J., Takemura, H., Thastrup, O., Leslie, B. A., and Putney, J. W. (1992) In situ imaging of agonist-sensitive calcium pools in AR4-2J pancreatoma cells. *J. Biol. Chem.* **267,** 25,568–25,575.
26. Connor, J. A. (1993) Intracellular calcium mobilization by inositol 1,4,5-trisphosphate, intracellular movements and compartmentalization. *Cell Calcium* **14,** 185–200.
27. Maltsev, V. A., Wolff, B., Hess, J., and Werner, G. (1994) Calcium signalling in individual T-cells measured by confocal microscopy. *Immun. Lett.* **42,** 41–47.
28. Trollinger, D. R., Cascio, W. E., and Lemasters, J. J. (1997) Selective loading of rhod-2 into mitochondria shows mitochondrial calcium transients during the contractile cycle in adult rabbit cardiac myocytes. *Biochem. Biophys. Res. Comm.* **236,** 738–742.
29. Zhao, M., Hollingworth, S., and Baylor, S. M. (1997) AM-loading of fluorescent calcium indicators into intact single fibers of frog muscle. *Biophys. J.* **72,** 2736–2747.
30. Tsien, R. Y. (1980) New calcium indicators and buffers with high selectivity against magnesium and protons, design, synthesis, and properties of prototype structures. *Biochem.* **19,** 2396–2404.
31. Bers, D. M., Patton, C. W., and Nuccitelli, R. (1994) A practical guide to the preparation of calcium buffers. *Methods in Cell Biology,* **40,** 4–29.
32. Fabiato, A., Fabiato, F. (1979) Calculator programs for computing the composition of the solutions containing multiple metals and ligands used for experiments in skinned muscle cells. *J. Physiol.* (Paris) **75,** 463–505.
33. Konishi, M., Olson, A., Hollingworth, S., and Baylor, S. M. (1988) Myoplasmic binding of fura-2 investigated by steady state fluorescence and absorbance measurements. *Biophys. J.* **54,** 1089–1104.
34. Hove-Madsen, L. and Bers, D. M. (1992) Indo-1 binding to protein in permeabilized ventricular myocytes alters its spectral and calcium binding properties. *Biophys. J.* **63,** 89–97.
35. Harkins, A. B., Kurebayashi, N., and Baylor, S. M. (1993) Resting myoplasmic free calcium in frog skeletal muscle fibers estimated with fluo 3. *Biophys. J.* **65,** 865–881.
36. Kurebayashi, N., Harkins, A. B., and Baylor, S. M. (1993) Use of fura red as an intracellular calcium indicator in frog skeletal muscle fibers. *Biophys. J.* **64,** 1934–1960.

37. Zhao, M., Hollingworth, S., and Baylor, S. M. (1996) Properties of Tri- and Tetra-carboxylate calcium indicators in frog skeletal muscle fibers. *Biophys. J.* **70,** 896–916.
38. Reers, M., Kelly, R. A., and Smith, T. W. (1989) Calcium and proton activities in rat cardiac mitochondria. *Biochem. J.* **257,** 131–142
39. Owen, C. S. (1991) Spectra of intracellular fura-2. *Cell Calcium* **12,** 385–393.
40. Bancel, F., Salmon, J.-M., Vigo, J., and Viallet, P. (1992) Microspectrophotometry as a tool for investigation of non-calcium interactions of Indo-1. *Cell Calcium* **13,** 59–68.
41. Bancel, F., Salmon, J.-M., Vigo, J., Vo-Dinh, T., and Viallet, .P (1992) Investigation of non-calcium interactions of fura-2 by classical and synchronous fluorescence spectroscopy. *Anal. Biochem.* **204,** 231–238.
42. Baker, A. J., Brandes, R., Schreur, J. H. M., Camacho, A., and Weiner, M. W. (1994) Protein and acidosis alter calcium binding and fluorescence spectra of the calcium indicator Indo-1. *Biophys. J.* **67,** 1646–1654.
43. Blatter, L. A. and Wier, W. G. (1990) Intracellular diffusion, binding and compartmentalization of the fluorescent calcium indicators indo-1 and fura-2. *Biophys. J*. **58,** 1491–1499.
44. Spurgeon, H. A., Stern, M. D., Baartz, G., Raffaeli, S., Hansford, R. G., Talo, A., Lakatta, E. G., and Capogrossi, M. C. (1990) Simultaneous measurement of calcium, contraction and potential in cardiac myocytes. *Am. J. Physiol.* H574–H586.
45. Erdahl, W. L., Chapman, C. J., Taylor, R. W., and Pfeiffer, D. R. (1994) Calcium transport properties of ionophores A23187, ionomycin and 4-BrA23187 in a well defined model system. *Biophys. J.* **66,** 1678–1693.
46. Kao, J. P. Y. (1994) Practical aspects of measuring calcium with fluorescent indicators. *Methods in Cell Biology* **40,** 155–181.
47. Mason, M. J. and Grinstein, S. (1993) Ionomycin activates electrogenic calcium influx in rat thymic lymphocytes. *Biochem. J.* **296,** 33–39.
48. Schnetkamp, P. P. M., Li, X.-B., Basu, D. K., and Szerencsei, R. T. (1991) Regulation of free cytosolic calcium concentration in the outer segments of bovine retinal rods by Na-Ca-K exchange measured with fluo 3. *J. Biol. Chem.* **266,** 2275–2292.
49. Kao, J. P. Y., Harootunian, A. T., and Tsien, R. Y. (1989) Photochemically generated cytosolic calcium pulses and their detection by fluo-3. *J. Biol. Chem*. **264,** 8179–8184.
50. Giovannardi, S., Cesare, P., and Peres, A. (1994) Rapid synchrony of nuclear and cytosolic calcium signals activated by muscarinic stimulation in the human tumour line TE571/RD. *Cell Calcium* **16,** 491–499.
51. Lin, C., Hajnoczky, G., and Thomas, A. P. (1994) Propagation of cytosolic calcium waves into the nuclei of hepatocytes. *Cell Calcium* **16,** 247–258.
52. Allbritton, N. L., Kuhn, O. E., and Meyer, T. (1994) Source of nuclear calcium signals. *Proc. Natl. Acad. Sci.* **9,** 12,458–12,462.
53. Shirakawa, H. and Miyazaki, S. (1996) Spatiotemporal analysis of calcium dynamics in the nucleus of hamster oocytes. *J. Physiol.* **494,** 29–40.

54. Perez-Terzic, C., Stehno-Bittel, L., and Clapham, D. E.(1997) Nucleoplasmic and cytoplasmic differences in the fluorescence properties of the calcium indicator Fluo-3. *Cell Calcium* **21,** 275–282
55. Neidle, S. and Abraham, Z. (1984) Structural and sequence-dependent aspects of drug intercalation into nucleic acids. *CRC Crit. Rev. Biochem*. **17,** 73–121.
56. Merritt, J. E., McCarthy, S. A., Davies, M. P., and Moores, K. E. (1990) Use of fluo-3 to measure cytosolic calcium in platelets and neutrophils. *Biochem. J.* **269,** 513–519.
57. Konishi, M. and Watanabe, M. (1995) Resting cytoplasmic free calcium concentration in frog skeletal muscle measured with fura-2 conjugated to high molecular weight dextran. *J. Gen. Physiol.* **106,** 1123–1150.
58. Fetcho, J. R. and O'Malley, D. M. (1995) Visualization of active neural circuitry in the spinal cord of intact zebrafish. *J. Neurophys*. **73,** 399–406.
59. Berlin, J. R. and Konishi, M. (1993) Calcium transients in cardiac myocytes measured with high and low affinity calcium indicators. *Biophys. J.* **65,** 1632–1647.
60. Eilers, J., Callewaert, G., Armstrong, C., and Konnerth, A. (1995) Calcium signaling in a narrow somatic submembrane shell during synaptic activity in cerebellar Purkinje neurons. *Proc. Natl. Acad. Sci.* **92,** 10,272–10,276.
61. Regehr, W. G. and Atluri, P. P. (1995) Calcium transients in cerebellar granule cell presynaptic terminals. *Biophys. J.* **68,** 2156–2170.
62. Birch, B. D., Eng, D. L., and Kocsis, J. D. (1992) Intranuclear calcium transients during neurite regeneration of an adult mammalian neuron. *Proc. Natl. Acad. Sci*. **89,** 7978–7982.
63. Cheng, H., Lederer, W. J., and Cannell, M. B. (1993) Calcium sparks, elementary events underlying excitation-contraction coupling in heart muscle. *Science* **262,** 740–744.
64. Stricker, S. A., Centonze, V. E., and Melendez, R. F. (1994) Calcium dynamics during starfish oocyte maturation and fertilization. *Dev. Biol*. **166,** 34–58.
65. Fetcho, J. R. and O'Malley, D. M. (1997) Imaging neuronal networks in behaving animals. *Curr. Opin. Neurobio.* **7,** 832–838.
66. Denk, W., Holt, J. R., Shepherd, G. M., and Corey, D. P. (1995) Calcium imaging of single stereocilia in hair cells, localization of transduction channels at both ends of tip links. *Neuron* **15,** 1311–1321.
67. Yuste, R. and Denk, W. (1995) Dendritic spines as basic functional units of neuronal integration. *Nature* **375,** 682–684.
68. Svoboda, K., Tank, D. W., and Denk, W. (1996) Direct measurement of coupling between dendritic spines and shafts. *Science* **272,** 716–719.
69. Berg, H. (1993) Random walks in biology. Princeton University Press, Princeton, NJ, pp. 34,35.
70. Al-Mohanna, F. A., Caddy, K. W. T., and Bolsover, S. R. (1994) The nucleus is insulated from large cytosolic calcium ion changes. *Nature* **367,** 754–750.
71. Przywara, D. A., Bhave, S. V., Bhave, A., Wakade, T. D., and Wakade, A. R. (1991) Stimulated rise in neuronal calcium is faster and greater in the nucleus than the cytosol. *FASEB J* **5,** 217–222.

72. Davis, M. A., Chang, S. H., and Trump, B. F. (1995) IP_3-mediated cytosolic and nuclear calcium elevation in NRK-52E cells using 'caged' $GPIP_2$. *Cell Calcium* **17,** 453–458.
73. Badminton, M. N., Campbell, A. K., and Rembold, C. M. (1996) Differential regulation of nuclear and cytosolic calcium in HeLa cells. *J. Biol. Chem.* **271,** 31,210–31,214.
74. Bkaily, G., Gros-Louis, N., Naik, R., Jaalouk, D., and Pothier, P. (1996) Implication of the nucleus in excitation contraction coupling of heart cells. *Molec. Cell. Biochem.* **154,** 113–121.
75. Ferrier, J. and Yu, H. (1996) Nuclear versus perinuclear and cytoplasmic calcium in osteoclasts. *Cell Calcium* **20,** 381–388.
76. Jovanovic, A., Lopez, J. R., and Terzic, A. (1996) Cytosolic calcium domain-dependent protective action of adenosine in cardiomyocytes. *Eur. J. Pharm.* **298,** 63–69.
77. Dani, J. W., Chernjavsky, A., and Smith, S. J. (1992) Neuronal activity triggers calcium waves in hippocampal astrocyte networks. *Neuron* **8,** 429–440.
78. Segal, M. and Manor, D. (1992) Confocal microscopic imaging of calcium in cultured rat hippocampal neurons following exposure to N-methyl-d-aspartate. *J. Physiol*. **448,** 655–676.
79. Kuba, K., Hua, S.-Y., and Hayashi, T. (1994) A UV laser-scanning confocal microscope for the measurement of intracellular calcium. *Cell Calcium* **16,** 205–218.
80. Grapengiesser, E. (1993) Cell photodamage, a potential hazard when measuring cytoplasmic calcium with fura 2. *Cell Struc. Func.* **18,** 13–17.
81. Lipp, P. and Niggli, E. (1993) Ratiometric confocal calcium-measurements with visible wavelength indicators in isolated cardiac myocytes. *Cell Calcium* **14,** 359–372.
82. Williams, R. M., Piston, D. W., and Webb, W. W. (1994) Two-photon molecular excitation provides intrinsic 3-dimensional resolution for laser-based microscopy and microphotochemistry. *FASEB J.* **8,** 804–813.
83. Kay, A. R. (1992) An intracellular medium formulary. *J. Neurosci. Meth.* **44,** 91–100.
84. Harrison, S. M. and Bers, D. M. (1987) The effect of temperature and ionic strength on the apparent Ca-affinity of EGTA and the analogous Ca-chelators BAPTA and dibromo-BAPTA. *Biochim. Biophys. Acta*. **925,** 133–143.
85. Williams, D. A. and Fay, F. S. (1990) Intracellular calibration of the fluorescent calcium indicator fura-2. *Cell Calcium* **11,** 75–83.
86. Baudet, S,. Hove-Madsen, L., and Bers, D. M. (1994) How to make and to use calcium-specific mini- and micro-electrodes. *Methods in Cell Biology* **40,** 94–113.
87. Becker, P. L. and Fay, F. S. (1987) Photobleaching of fura-2 and its effect on determination of calcium concentrations. *Am. J. Physiol.* **253,** C613–C618.
88. Moore, E. D. W., Becker, P. L., Fogarty, K. E., Williams, D. A., and Fay, F. S. (1990) Calcium imaging in single living cells, theoretical and practical issues. *Cell Calcium* **11,** 157–179.
89. Stevens, T., Fouty, B., Cornfield, D., and Rodman, D. M. (1994) Reduced PO_2 alters the behavior of fura-2 and indo-1 in bovine pulmonary artery endothelial cells. *Cell Calcium* **16,** 404–412.

90. Lattanzio, F. A. and Bartschat, D. K. (1991) The effect of pH on rate constants, ion selectivity and thermodynamic properties of fluorescent calcium and magnesium indicators. *Biochem. Biophys. Res. Comm.* **177,** 184–191.
91. Matthews, G. G. (1991) Cellular physiology of nerve and muscle. Blackwell Scientific Publications, Cambridge, MA.
92. Hille, B. (1992) Ionic channels of excitable membranes. Sinauer Associates, Sunderland, MA.
93. Johnston, D .and Wu, S. S.-M. (1995) Foundations of cellular neurophysiology. MIT Press, Cambridge, MA.
94. Sherman-Gold, R. (Ed.) (1993) The Axon Guide. Axon Instruments, Foster City, CA.
95. Lopez ,H. S. (1992) Kinetics of G protein-mediated modulation of the potassium M-current in bullfrog sympathetic neurons. *Neuron* **8,** 725–736.
96. Jones, S. W. (1987) Sodium currents in dissociated bull-frog sympathetic neurones. *J. Physiol.* **389,** 605–627.
97. Toescu, E. C., Lawrie, A. M., Gallacher, D. V., and Petersen, O. H. (1993) The pattern of agonist-evoked cytosolic calcium oscillations depends on the resting intracellular calcium concentration. *J. Biol. Chem.* **268,** 18,654–18,658.
98. Sala, F. and Hernandez-Cruz, A. (1990) Calcium diffusion modeling in a spherical neuron, relevance of buffering properties. *Biophys. J.* **57,** 313–324.
99. Nowycky, M C. and Pinter, M. J. (1993) Time course of calcium and calcium-bound buffers following calcium influx in a model cell. *Biophys. J.* **64,** 77–91.
100. Sobierajski, L., Avila, R., O'Malley, D. M., Wang, S., and Kaufman, A. (1995) Visualization of calcium activity in nerve cells. *Computer Graphics Appl.* **15,** 55–61.
101. Berlin, J. R., Bassani, J. W. M., and Bers, D. M. (1994) Intrinsic cytosolic calcium buffering properties of single rat cardiac myocytes. *Biophys. J.* **67,** 1775–1787.
102. Zhou, Z. and Neher, E. (1993) Mobile and immobile calcium buffers in bovine adrenal chromaffin cells. *J. Physiol.* **469,** 245–273.
103. Neher, E. (1995) The use of fura-2 for estimating calcium buffers and calcium fluxes. *Neuropharm.* **34,** 1423–1442.
104. Mize, R. R., Luo, Q., Butler, G., Jeon, C. J., and Nabors, B. (1992) The calcium binding proteins parvalbumin and calbindin-D 28K form complementary patterns in the cat superior colliculus. *J. Comp. Neurol*. **320,** 243–256.
105. Peters, R. (1984) Nucleocytoplasmic flux and intracellular mobility in single hepatocytes measured by fluorescence microphotolysis. *EMBO J.* **3,** 1831–1836.
106. Peters, R. (1986) Fluorescence microphotolysis to measure nucleocytoplasmic transport and intracellular mobility. *Biochim. Biophys. Acta*. **864,** 305–359.
107. Csermely, P., Schnaider, T., and Szanto, I. (1995) Signalling and transport through the nuclear membrane. *Biochim. Biophys. Acta* **1241,** 425–452.